Summer 2017

Functionalization of Indium-Based Quantum Dots for Use as a Non-Viral Gene Therapy Vector

Nicholas A. Mundt
Missouri State University, Mundt711@live.missouristate.edu

FUNCTIONALIZATION OF INDIUM-BASED QUANTUM DOTS FOR USE AS A NON-VIRAL GENE THERAPY VECTOR

A Masters Thesis

Presented to

The Graduate College of

Missouri State University

In Partial Fulfillment

Of the Requirements for the Degree

Master of Science, Chemistry

By

Nicholas A. Mundt

August 2017

FUNCTIONALIZATION OF INDIUM-BASED QUANTUM DOTS FOR USE AS A NON-VIRAL GENE THERAPY VECTOR

Chemistry

Missouri State University, August 2017

Master of Science

Nicholas A. Mundt

ABSTRACT

This work aims to develop functionalized, water-soluble indium-based quantum dots (QDs) as a non-viral gene therapy vector. The QDs were solubilized in water by exchanging native hydrophobic surface ligands with 11-mercaptoundecanioc acid (MUA); an amphiphilic ligand providing terminal carboxylate groups that impart water solubility to the QDs. The aqueous QDs were then functionalized with a terminal tertiary amine to impart a positive surface charge, allowing negatively-charged DNA to complex with the nanoparticles. The QDs were characterized via electrophoresis to determine their ability to bind DNA. Results show that further work is needed to optimize DNA binding. In addition, this work explores QD bioconjugation with lactose as an intracellular targeting molecule, to direct QD complexes to the cellular nucleus. Conjugation with lactose was confirmed via nuclear magnetic resonance (NMR) spectroscopy. QD probes trafficking in N2a (mouse neuroblastoma) cells was visualized using fluorescence microscopy and immunocytochemistry (ICC). The images were analyzed via Manders' coefficient to determine the degree of QD colocalization with different organelles inside the cell. Results proved inconclusive due to instrumental limitations.

KEYWORDS: quantum dots, gene therapy, bioconjugation, fluorescence microscopy, confocal microscopy

This abstract is approved as to form and content

_____

Katye M. Fichter, Ph.D.
Chairperson, Advisory Committee
Missouri State University

FUNCTIONALIZATION OF INDIUM-BASED QUANTUM DOTS FOR USE AS A NON-VIRAL GENE THERAPY VECTOR

By

Nicholas A. Mundt

A Masters Thesis
Submitted to the Graduate College
Of Missouri State University
In Partial Fulfillment of the Requirements
For the Degree of Master of Science, Chemistry

August 2017

Approved: _____
Katye M. Fichter, Ph.D.

_____
Reza Sedaghat-Herati, Ph.D.

_____
Keiichi Yoshimatsu, Ph.D.

_____
Kyoungtae Kim, Ph.D.

_____
Julie Masterson, Ph.D.: Dean, Graduate College

ACKNOWLEDGEMENTS

There are many people I would like to acknowledge and thank for their help and support during my graduate studies. First, Dr. Katye Fichter, my advisor, for all her help and support throughout this process. From undergraduate to graduate school she has mentored and helped me throughout it all. Dr. Reza Herati, no matter when or how many times I showed up to his office unannounced, he made time to help and advise me in many different aspects of this work. As a teaching assistant, he was a wonderful coordinator to work with and made my time teaching very enjoyable. Dr. Keiichi Yoshimatsu, for use of his peptide synthesizer, it provided great experience for me. Dr. Kyoungtae Kim, for use of your confocal microscope, it was paramount to these studies. Matt Ellis, for helping me with so much during my time here. It did not matter if it was related to class or research, you were always available for help or ideas, even if some of your ideas were a little crazy. I would like to say thanks, Obama, for your belief in the need for science and funding it. Also, thank you to all my lab mates in the Fichter lab, past or present, you have all helped me succeed in some way or another. Finally, I would like to thank all my friends and family for your support.

TABLE OF CONTENTS

LIST OF FIGURES

CHAPTER 1: INTRODUCTION

1.1 Quantum Dots

Quantum Dots (QDs) are small semiconducting nanocrystals ranging in size from 2-20 nanometers (nm) that fluoresce brightly when irradiated with ultraviolet or visible light[1]. QDs are typically composed of group II and VI, or group III and V elements[2]. There are a number of unique advantages to QDs including their small size, size-tunable emission wavelength, and increased photostability compared to organic dyes. Current work with QDs include applications in solar cells, photodetectors, LEDs, medical diagnostics and therapeutics[1,3,34,35]. The ability to carefully control surface characteristics and functionality of QDs makes them an excellent choice for use in biomedical applications.

When irradiated with UV light, electrons in the QD become excited. The excited electrons create an exciton pair consisting of an electron and a positive hole. There are several modes of relaxation the electron can undergo (Figure 1.1). If the electron recombines with the hole, then a photon is released (*i.e.* fluorescence). This path is known radiative relaxation. There are several ways that allow the electron to relax without emitting a photon, collectively known as non-radiative relaxation. These include relaxation of vibrational or rotational modes and intersystem crossing. If the electron undergoes non-radiative relaxation, it can cause the formation of a surface defect, leading to trap states. Trap states cause a decrease in overall fluorescence and quantum yield of the QDs. In order to protect the QDs from trap states and surface defects a core/shell structure is typically employed.

Currently, the most popular QD core/shell system used is cadmium selenide/zinc sulfide (CdSe/ZnS). CdSe QDs exhibit intense fluorescence and narrow emission peak widths[39]. Their use in biomedical applications does have some concern due the toxicity of Cd^{2+} ions that may be released through degradation of the QD[40]. Other core systems can be employed to increase biocompatibility of the QDs. In this study, indium-based QDs were used, specifically indium phosphide/zinc sulfide, because they possess similar characteristics of cadmium-based QDs without the toxicity of Cd^{2+} ions[41]. Indium-based QDs have lower quantum yield and broader emission peaks, yet are still being used in biomedical applications despite these characteristics[43].

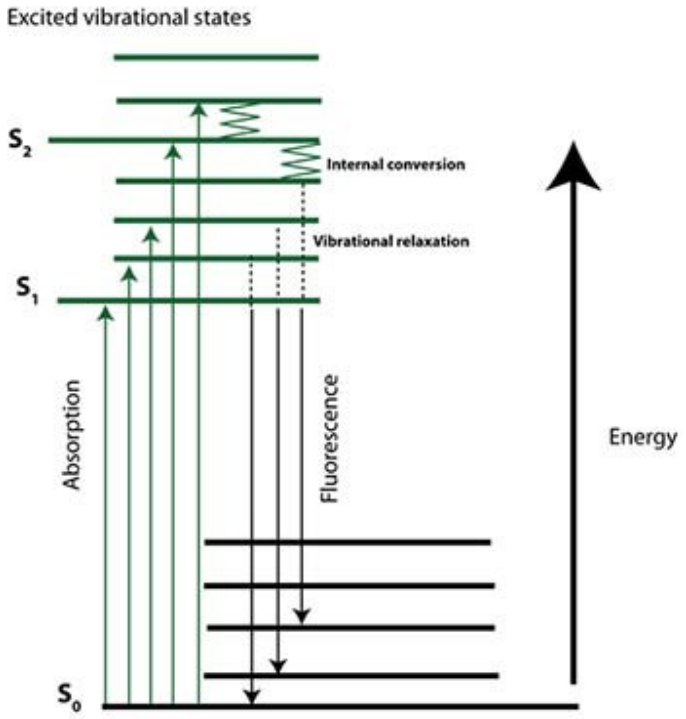

Figure 1.1. Jablonski diagram[7]. The Jablonski diagram shows different methods of relaxation for an excited electron.

The fluorescence property of QDs comes from the size of the QD itself. Typical indium phosphide (InP) QDs range in size from 2-6 nm[4]. The fluorescent properties of QDs come from the fact that they are smaller in size than the exciton Bohr radius. The exciton Bohr radius is defined as the distance between an excited electron and the hole left behind after excitation. The result is that the energy levels within the QD become discrete, quantized levels and no longer exhibit continuous bandgap properties like bulk semiconductors. Another effect of the QD size is a property known as quantum confinement in which the band gap of the QDs increase as their physical size decreases[5]. Smaller QDs fluoresce toward the blue end of the spectrum while larger QDs are more red shifted (Figure 1.2). This allows for size-tunable emission wavelengths that can be tailored to fit the experiment at hand.

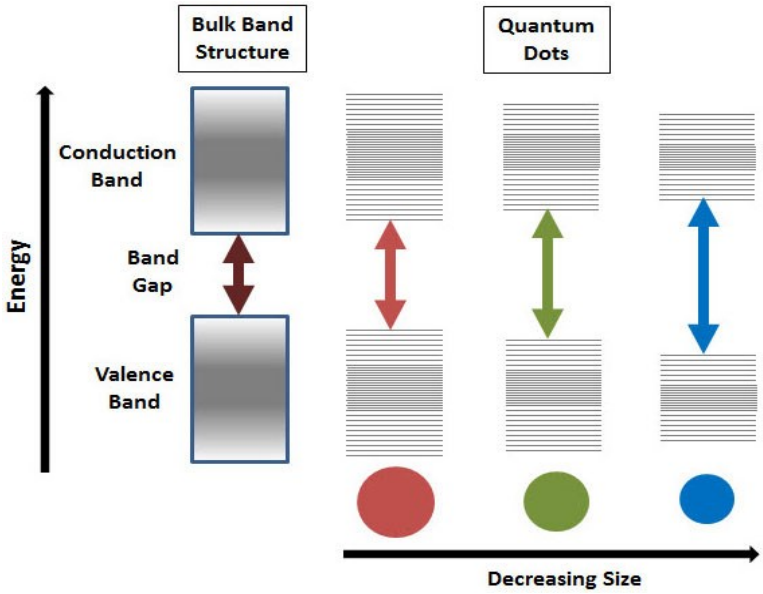

Figure 1.2. Size-tunable emission of quantum dots[6]. The emission wavelength of QDs depends on the QD size. Quantum confinement allows for discrete energy levels unlike bulk semiconductors. The size of the QD and its band gap have an inversely proportional relationship. As the size of the QD increases, the band gap increases resulting in a red shifted emission wavelength.

The core of the QD is susceptible to oxidative degradation as well as the surface defects mentioned above. When exposed to UV light in the presence oxygen, the cores undergo oxidation[8] (Figure 1.3). The oxidation reduces the overall size of the QD and can be observed as a blue shifting of the emission fluorescence. If the QDs continue to degrade they will eventual cease to fluoresce. In order to prevent surface oxidation, a shell is added around the QD core to protect it. Typical shells are composed of zinc and sulfur, coating the QD core with about 3-6 monolayers of zinc sulfide (ZnS).

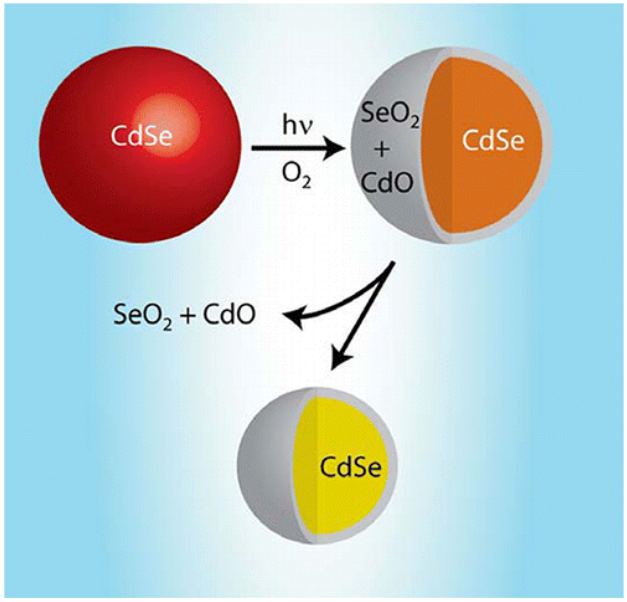

Figure 1.3[8]. An example of the process of oxidative degradation of CdSe QD cores. When exposed to oxygen and UV light, the QD cores can oxidize. Oxidation of the cores can manifest as a blue shifting in fluorescence emission (due to the size decrease in the QD size) and/or dimming of the fluorescence intensity.

After synthesis, the QDs have hydrophobic surface ligands, rendering them insoluble in water. To be useful in many applications (*e.g.* biomedical applications) the QDs must to be soluble in water. There are three major methods used to impart water solubility: which include 1) silica encapsulation, 2) polymer encapsulation, and 3) ligand exchange.

Each method has advantages and disadvantages in terms of stability, size increase, and technical effort needed.

Silica encapsulation involves depositing a layer of SiO_2 around the QD core. Typically, silica precursors are added after core growth to encapsulate the QD and leave the hydrophilic SiO_2 on the surface[9]. The silica coating of the QD not only provides water solubility but excellent protection of the core including in acidic environments. The downside to silica encapsulation is the uneven coating of silica around the QDs[32]. Variable size distribution pose issues in some applications.

Another method of solubilization is polymer encapsulation. In this method, the native hydrophobic ligands on the QD surface are used along with an amphiphilic polymer to impart water solubility. Trioctylphosphine oxide (TOPO) is a hydrophobic ligand often used in QD synthesis and therefore is often found on the QD surface after synthesis. Other surface ligands may include long chain amines or thiols such as oleylamine or dodecanethiol, respectively. The amphiphilic polymer contains both hydrophobic and hydrophilic moieties. The hydrophobic moieties of the polymer interact with the native hydrophobic ligands on the QD surface while the hydrophilic moieties are exposed to the solvent (Figure 1.4). The hydrophilic surface now provides water solubility for the QDs. The amphiphilic polymer can contain chemical handles such as carboxyl or amine groups to allow for further modification or bioconjugation of the QD. The large polymer allows for a lot of interaction between itself and the QD which, in turn, provides good stability in solution over time. Disadvantages of the polymer encapsulation method include the increased size of the QDs, and the possibility of encapsulating multiple QDs together. That is, with the large polymers typically used in

this reaction, it is possible to wrap multiple QDs together instead of creating single encapsulated QDs.

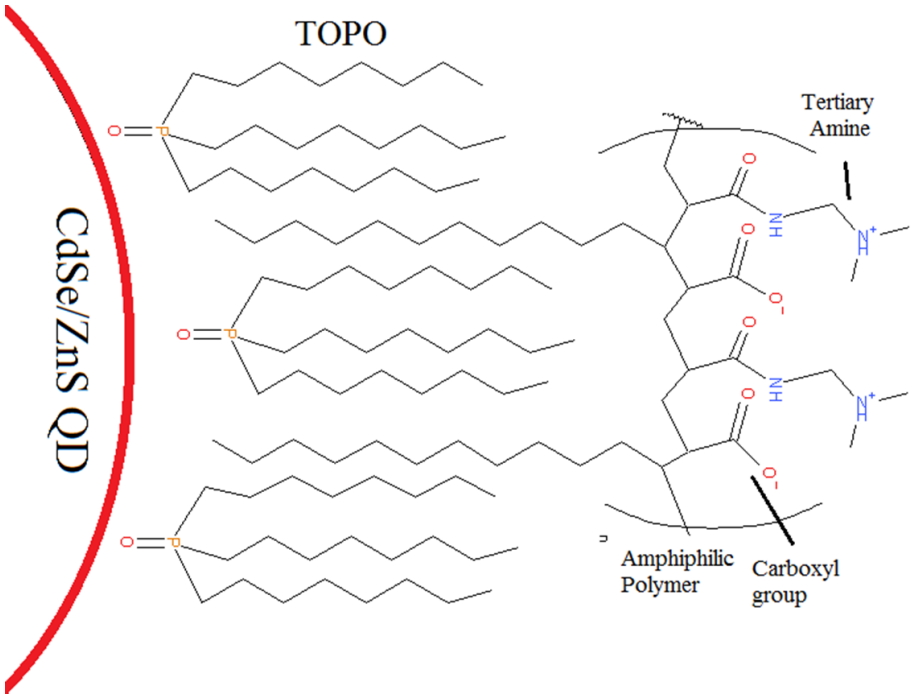

Figure 1.4. Water solubilization of QDs via polymer encapsulation. The native ligands on the QD surface interact with the hydrophobic portion of the amphiphilic polymer in order to impart water solubility to the QDs. The exposed hydrophilic portion of the polymer contains various chemical handles the can be used to further modify the QDs.

Another method of water solubilization is ligand exchange. The native hydrophobic ligands on the QD are datively bonded to the QD surface. In ligand exchange, amphiphilic ligands are introduced to compete for binding on the QD surface (Figure 1.5-1.6). Thiols are often used because they bind well to zinc in the QD shell. The sulfur in the thiol ligands forms a stronger bond than the oxygen of TOPO, causing the TOPO ligands to be replaced. There are several commonly used thiol ligands including 3-mercaptopropanoic acid (MPA), 11-mercaptoundecanoic acid (MUA), and dihydrolipoic (DHLA). Both MPA and MUA are monovalent ligands, meaning that each ligand has one

binding spot. One of the downfalls of ligand exchange is the decreased long term stability in solutions. The ligands can dissociate from the QDs over time resulting in a loss of water solubility. It is possible to avoid this effect by using multidentate ligands, such as DHLA, which has two sulfur atoms. Additionally, some research groups have reported using tetradentate sulfur ligands to further increase the long-term water solubility of QDs[10]. The resulting QDs after ligand exchange a much smaller size than polymer-encapsulated QDs. This is key for applications that need the small size of QDs to be effective. The biggest advantage of ligand exchange over the other techniques is that the surface chemistry of the QDs can be highly controlled. This leads to more uniform QDs without variations in size or surface moieties.

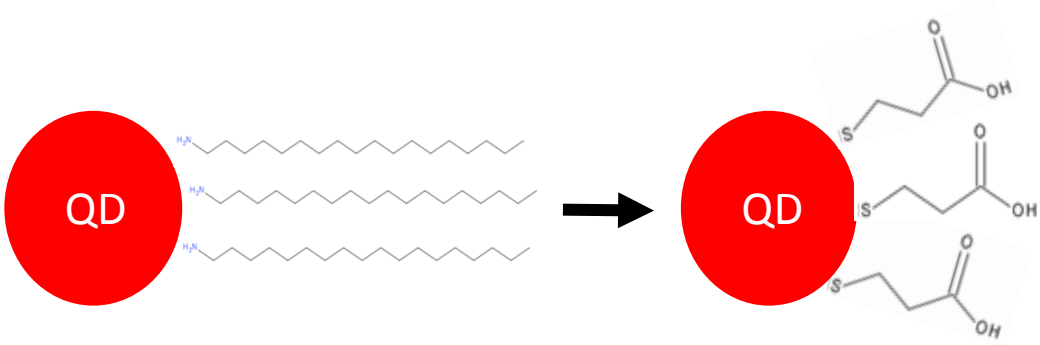

Figure 1.5. Water solubilization of QDs via ligand exchange. The native hydrophobic ligands on the QD surface are exchanged for hydrophilic ligands in a biphasic reaction. The terminal ends of the new ligands allow for further chemical modification as well as imparting water solubility. This example shows native oleylamine ligands being exchanged with MPA.

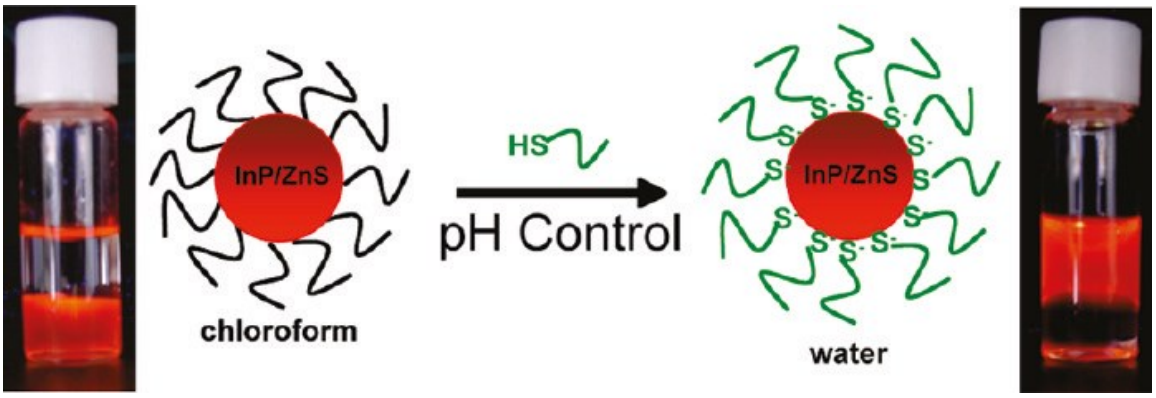

Figure 1.6. Ligand exchange phase transfer of QDs[27]. As the solution stirs, native QD ligands exchange for hydrophilic ligands in the aqueous layer. Overtime all the QDs move from the bottom organic layer to the upper aqueous layer.

1.2 Gene Therapy

Gene therapy is a powerful tool that has been used in an attempt to treat many genetic diseases[11,12]. Gene therapy uses a delivery vector to deliver therapeutic DNA to cells to replace missing or mutated genes. Viruses are a common vector in gene therapy because of their innate ability to deliver DNA into cells. There are also many non-viral techniques being researched due to the safety concerns of using viral vectors[13].

Currently, the most common therapeutic technique is viral gene therapy. Many types of viruses are used; retroviral vectors are the most common of all viral vectors[12]. In order for the virus to safely deliver the therapeutic gene, the genome of the virus is modified to remove infectious or damaging DNA sequences. Even though viral vectors are extremely efficient at delivering DNA, there are a number of safety concerns associated with them. One of the first clinical trials using viral gene therapy was conducted in 1992 in Italy for the treatment of hereditary diseases. Many years after treatment, patients began suffering from leukemia, and concerns over the safety of gene

therapy were raised[11,12]. Many viral gene therapy clinical trials were temporarily halted until safety concerns could be addressed[36,37,38]. The problem is that even though viral vectors could deliver the DNA there was no way to control where the DNA was inserted into the patients genome. Improper insertion of the exogenous DNA could lead to the disruption of healthy gene expression[12]. For example, if a gene controlling the cell cycle was disrupted, the cell could become cancerous.

There are a number of non-viral gene therapy methods that have been explored as a way to alleviate some safety issues of using viral vectors. Lipoplexes or polyplexes are materials that are used to deliver therapeutic DNA. These vectors condense and protect DNA with the respective organic complexing agent. Lipoplexes are cationic lipids that electrostatically interact with DNA and cause condensation of DNA with the lipid. The lipid:DNA complex is thought to enter the cell through endocytosis where it must then diffuse into the cytosol[14,15]. Polyplexes work in a similar way except they involve using a positively charged polymer (*e.g.* polyethylenimine, PEI) to complex the DNA. Polyplexes tend to be amorphous in shape and polydisperse in size, causing them to be more difficult to characterize. QDs that are inherently positively charged are a possible solution to the irregularity of lipoplexes and polyplexes.

Although non-viral vectors are safer than their viral counterparts, there are still several issues that must be overcome. Non-viral vectors are not nearly as efficient at delivering DNA to the nucleus of a cell. The most common method of entry into the cell is through endocytosis[16]. Two types of endocytosis, clathrin-mediated or caveolin-mediated, are believed to be the major ways in which the vectors are internalized. Upon internalization, the vectors are in vesicles known as endosomes. The exogenous material

is sorted into specific vesicles, depending on the identity of the material, and then vesicles are trafficked through different routes in the cell. The least favorable outcome for therapeutic DNA is trafficking to the lysosomes. Lysosomes have a low pH (*e.g.* 4-5) and contain nucleases that will degrade any therapeutic DNA. In order to avoid lysosomal trafficking of the therapeutic DNA, there needs to be a way to direct the trafficking away from the lysosomes (*e.g.* via a targeting molecule). Previous work has shown non-viral vectors that incorporate sugar molecules may be trafficked toward the Golgi[31]. This is promising because the lumen of the ER is contiguous with the space between the inner and outer nuclear membranes

The use of QDs as a non-viral vector allows for a great variety of surface modifications to mediate cellular uptake and trafficking. Molecules can be conjugated to the QDs to act as targeting agents or change the chemistry of the surface (*e.g.* reducing surface charge). This work explores the use of lactose as a targeting agent and the addition of poly(ethylene) glycol (PEG) polymers to increase uptake and reduce non-specific binding[17,18].

1.3 Lactose and Galectin-3

Lectins are carbohydrate-binding proteins found in plants and animals. There are a number of different lectins in mammalian cells but galectin-3 is of particular interest to this work. Galectin-3 is a 31 kDa protein that specifically binds β-galactosides[19,20] (*i.e.* sugars containing galactose). The majority of galectin-3 is located within the cytoplasm of the cell but some cell types can also express a significant amount within the nucleus[19,21]. Galectin-3 had been shown to enter the nucleus of cells via passive diffusion

as well as active transport[33]. A six amino acid sequence in the protein acts as a nuclear localization sequence allowing for active transport through the nuclear pore.

One common β-galactosides is lactose. Lactose is a disaccharide composed of a glucose and galactose sugar. Galectin-3 exhibits a high affinity for lactose and N-acetyllactosamine[19,21]. Lactose can be conjugated to the QD through the use of chemical handles on the QD surface (*i.e.* carboxylate groups). The alcohol groups of the lactose can be reacted with the carboxylate groups on the QD surface to form stable ester bonds. We propose using lactose as a targeting molecule to help deliver QD:DNA conjugates to galectin-3. The complex may be trafficked toward the nucleus of the cell using native cellular trafficking.

1.4 Cell Culture

In order to perform the *in vitro* studies employed in this project, it was necessary to maintain stable cell lines of mammalian cells. All work with these cells needs to be performed in a sterile environment to prevent contamination. Equipment and solutions must be kept sterile; therefore, all cell culture studies were done in a bio-safety cabinet. An autoclave was used to sterilize all hardware used in cell culture experiments. Disposables (*e.g.* cell flasks, pipette tips, etc.) brought into the bio-safety hood were wiped with a 75% ethanol solution to ensure proper sanitation. Cells were kept in an incubator at a constant 37 °C to ensure optimal growth. A bicarbonate-buffered media was used to maintain a constant pH in the cell culture flask; therefore, the incubator also maintained an atmospheric concentration of CO_2 at 5 %. The presence of phenol red in the cellular media allows quick assessment by color to roughly indicate the pH. It is a

bright pink color above pH 8.2; red at physiological pH, and orange-yellow as the pH approaches 6.8. Proper techniques must be used to ensure viability of the cells for use in cellular studies.

The N2a (mouse neuroblastoma) cell line was used in cellular studies discussed herein. The cells were grown in cell culture flasks and split every 2-3 days to maintain healthy growing conditions. If the cells become overly confluent they begin growing on top of each other instead of in a single monolayer. This may cause differentiation and changes in cellular morphology, which would complicate the analysis of intracellular trafficking. In overconfluent cells, selective pressure causes the cells best suited to grow in unhospitable environments to thrive. The resulting cells no longer represent the model cell line that was initially chosen. It is important for the cells to retain the characteristics of the chosen model cell line.

1.5 Microscopy

Microscopy has long been used to study objects which are too small to be seen. Light microscopy is a specific type in which visible light is used to detect the sample. There are a number of different types of light microscopies, including phase-contrast (PC), differential-interference-contrast (DIC), epifluorescence, and confocal microscopy. Each type has specific uses along with respective advantages and disadvantages.

DIC microscopy is a type of brightfield microscopy used to enhance contrast in transparent samples such a mammalian cells. In DIC microscopy light first hits a 45° polarizing lens followed by a Wollaston prism[22]. This prism causes the polarized light to separate into two orthogonal rays. The two rays then hit a condenser lens that focuses the

light onto the sample. The two orthogonal rays will have different optical path lengths depending on the refractive index of the sample they are passing through. Once the light leaves the sample it passes through the objective lens and a second Wollaston prism. This causes the two orthogonal rays of light to recombine. The recombination of light causes interference, either constructive or destructive, that brightens or darkens parts of the image. Figure 1.7 shows the complete optical path used in DIC microscopy.

Epifluorescence microscopes are similar to compound microscopes but includes a fluorescence light source (*e.g.* mercury arc lamp) and a set of filter cubes. The filter cubes are composed of an excitation filter, dichroic mirror, and emission filter (Figure 1.8). The excitation filter only allows a narrow range of wavelengths through that correspond with the excitation wavelength of the fluorophore. Once passed through the excitation filter the light is reflected off a dichroic mirror towards the sample. A dichroic mirror reflects light under a certain wavelength and allows wavelengths above the cutoff to go through.

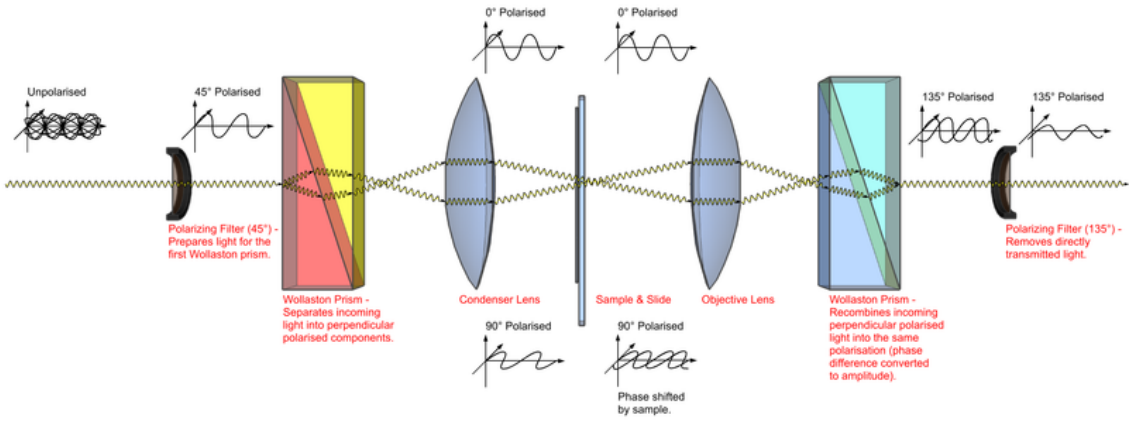

Figure 1.7. Light path in DIC microscopy[23]. This image shows the light path during DIC microscopy. Unpolarized light first hits a polarizing lens resulting in 45° polarized light. The light then hits a Wollaston prism separating it into two orthogonal rays. A condenser lens focuses the light through the sample. An objective lens focuses the light coming through the sample onto a second Wollaston prism which leads to a final polarizing lens.

This light is then directed towards and irradiates the sample on the microscope stage and excites electrons of the fluorophores in the sample. The emitted light from the fluorophore that is directed towards the objective travels back towards the dichroic mirror and through an emission filter that removes any stray light. Each fluorophore that is visualized needs its own set of filters. This allows many different fluorophores to be visualized in one sample without overlap.

Confocal microscopy is a powerful tool that is often used to study biological samples, such as cells. The light source used in confocal microscopy is a laser. Laser light has a very narrow wavelength bandwidth, making it excellent for exciting specific fluorophores. In normal fluorescence microscopy, the sample is irradiated with light evenly throughout. Confocal microscopy makes use of two spatial pinholes that block out of focus light (Figure 1.9). The result is that the only light detected originates from one

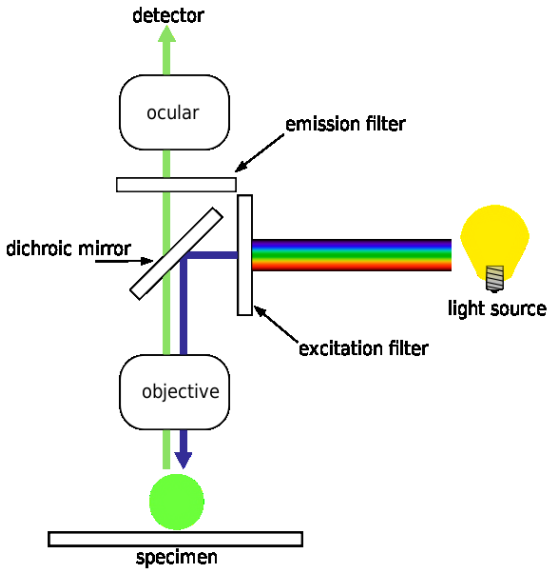

Figure 1.8. Filter cube for fluorescent microscopes[24]. This figure shows the light path through a filter cube. An excitation filter only allows the specified wavelength through. A dichroic mirror directs light toward the sample. Light emitted from the sample travels through the dichroic mirror and through an emission filter to the objective.

focal plane of the sample. A stage controller can be used to make very small focal plane "steps" up through the cell at increments as low as 400 nm and record many image planes, which collectively are known as a z-stack of the sample. These images can be processed to create a 3D image of the sample (Figure 1.10).

In order to determine if two different signals come from the same location in the sample co-localization analysis must be done. A number of different analyses have been developed to determine the co-localization between the signal detected for two different fluorophores in a sample.[26] (*e.g.* Pearson's correlation coefficient and Manders' overlap coefficient). There are advantages and drawbacks of each technique; therefore, it is critical to choose one best suited to the sample and the analysis performed. For this work, Manders' co-localization coefficient (MCC) was used to determine the degree of overlap between the signals detected between the QDs and an organelle fluorescently labeled in the cell. The overlap between two fluorophores (*e.g.* red and green) can be expressed as two different equations in MCC analysis:

$$M_1 = \frac{\sum R_{i,coloc}}{\sum R_i}$$

$$M_2 = \frac{\sum G_{i,coloc}}{\sum G_i}$$

M_1 denotes the fraction of red (R) pixels that overlap with green pixels, while M_2 denotes the fraction of green (G) pixels that overlap with red pixels[26]. In this study, QDs fluoresce red and cellular organelles of interest were labeled green. For this reason, analysis herein uses M_1 to indicate the overlap of QDs with the organelle of interest. That is, QD-containing pixels that overlap with organelle-labeled pixels is the objective of the colocalization analysis, not the overlap of organelle-labeled pixels that overlap with QD

pixels (*i.e.* we are most interested in the presence and location of QDs, not the presence and location of organelles).

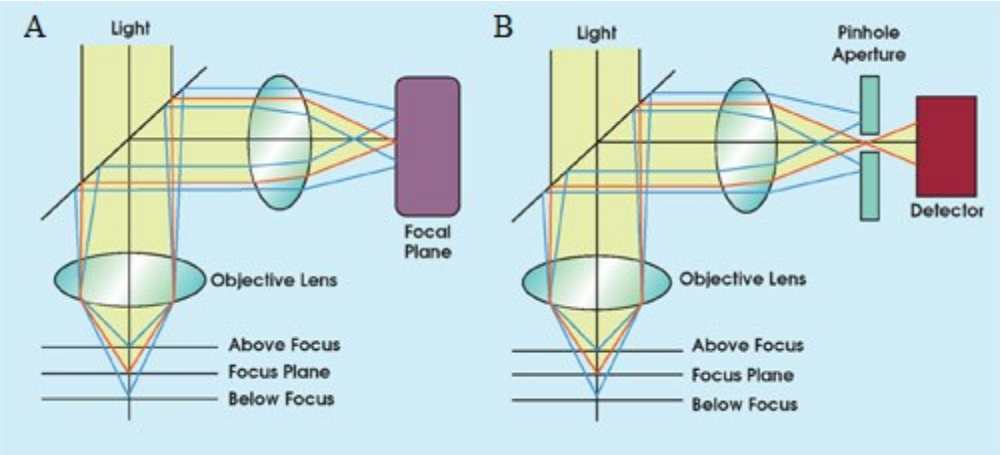

Figure 1.9. Light path comparison of conventional and confocal microscopy[44]. (A) Conventional microscopy allows light from different planes to be visualized at once. (B) Confocal microscopy makes use of two pinholes that block all background light. Only light from the plane being observed passes through to the detector. This allows for many planes to be imaged and formed into a 3D image.

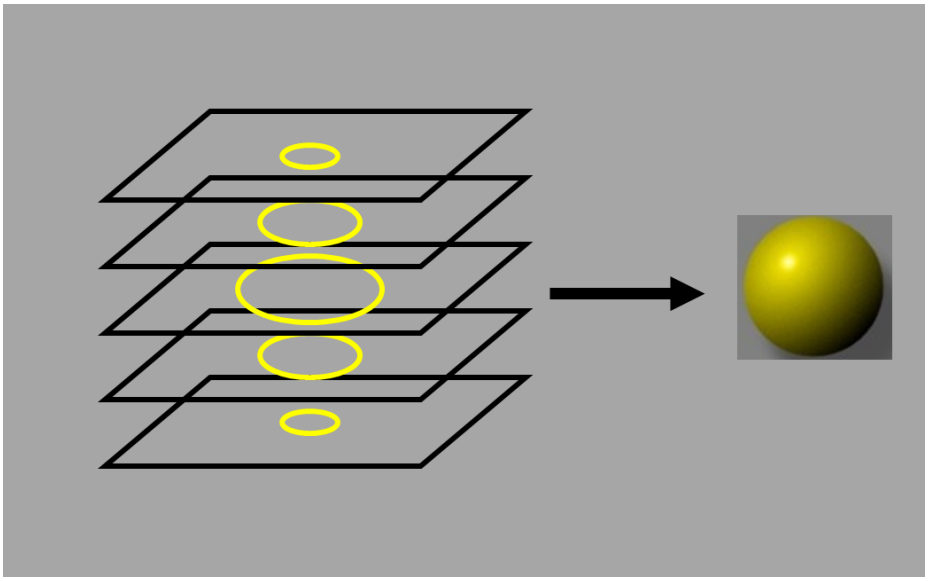

Figure 1.10. Z-Stacking[25]. Using confocal microscopy it is possible to take images of a number of different planes in the sample. Software can be used to merge the image (z-stacks) into a 3D image of the sample.

CHAPTER 2: EXPERIMENTAL

2.1 Chemical List

All chemicals were purchased from Sigma-Aldrich and used as is unless specified otherwise. Agarose (MidSci, Cat. No. Be-A125), 3-(dimethylamino)-1-propylamine (Cat. No. D158003), 4-(4,6-dimethoxy-1,3,5-triazin-2-yl)-4-methylmorpholinium chloride (DMTMM) (Cat. No. 749613), hexanes (EMD Millipore, Cat. No. 110-54-3), 3-(N-morpholino) propanesulfonic acid (MOPS) (Fisher, Cat. No. BP308-500), paraformaldehyde (PFA) (Cat. No. 158127), poly(ethylene glycol) derivatives ((Creative PEGworks, H_2N-PEG_{2000}-CH_3 ("mPEG") (Cat. No. PLS-269), H_2N-PEG_{2000}-COOH ("cPEG") (Cat. No. PLS-930)), Triton X-100 (Astoria Pacific, Cat. No. 90-0770-04), boric acid (Cat. No. B7901), sodium tetraborate decahydrate (Cat. No. S9640), 11-mercaptoundecanoic acid (MUA) (Cat. No. 450561 and Chem Cruz, Cat. No. sc-251618), tetramethyl ammonium hydroxide (TMAH) (Acros, Cat. No. 207520250), acetone (Fisher, A1320), Toluene (Fisher, T324), ethanol (Ultra Pure, Cat. No. 16A4E), 20K MWCO dialysis units (Fisher, Cat. No. 69590).

For cell culture and subsequent immunocytochemistry, the following reagents were used. Dulbecco's-Modified Eagle's medium (D-MEM) (Thermo Scientific, Cat. No. SH30022.01), Opti-MEM reduced serum medium (Life Technologies, Cat. No. 51985-034), rabbit anti-giantin antibody (Golgi Apparatus Marker, Abcam, Cat. no. ab24586), rabbit anti-lamin antibody (Nuclear envelope marker, Abcam, Cat. No. ab16048), rabbit anti-GRP78 BiP antibody (Endoplasmic reticulum marker, Abcam, Cat. No. ab21685), rabbit anti-Rab5 antibody (Endosome marker, cell signaling tech., Cat. No. 35478), rabbit

anti-lamp1 antibody (Lysosome marker, Abcam, Cat. No. ab24170), anti-rabbit Alexa488 conjugated antibody (Life Technologies, Cat. No. A21441), fetal bovine serum (Hyclone, Cat. No. SH30396.02) antibiotic/antimitotic solution 100X (Penicillin G, Streptomycin, and Amphotericin B) (Hyclone, Cat. No. SV30079.01), trypsin (Hyclone, Cat. No. AV30031.01), trypan blue (Hyclone, Cat. No. AV30084.01) and SYBR® Safe (Life Technologies, Cat. No. S-33102), 12 well plate (Corning, Cat. No. 353043), 18mm coverslips (Fisher, Cat. No. 12-545-84), N2a (mouse neuroblastoma) cells were a kind gift provided by Dr. Tania Q. Vu at Oregon Health and Science University.

2.2 Water Solubilization of QDs

After synthesis, QDs are only soluble in organic solvents (*e.g.* hexanes). To be useful in biological applications the QDs need to be soluble in water. There are several different approaches that can be used, as previously discussed in Chapter 1.1. Studies herein used ligand exchange to impart water solubility on the QDs.

Early attempts at water solubilization were conducted using dihydrolipoic acid (DHLA) as the solubilizing ligand. Lipoic acid had to be reduced to DHLA before being useful for water solubilization. Lipoic acid (1 g) was dissolved in 0.25 M sodium bicarbonate buffer. Slowly, 1.1 molar equivalent of sodium tetraborohydride was added and allowed to react for 1 hour. The solution was then acidified with 1 M HCl and the DHLA was extracted using chloroform. The chloroform was removed via rotovap leaving DHLA. Before beginning, the QDs were washed to remove any excess hydrophobic ligands in solution after synthesis. For washing, 1 mL of acetone was added to approximately 500 μL of 7 μM QDs (obtained from Matt Ellis, notebook number MAE-

001-45) in a 1.5 mL Eppendorf tube. The solution is then spun in a centrifuge at 5000 x g for 5-10 minutes, causing precipitated QDs to form a pellet at the bottom of the tube. The supernatant was discarded and the pellet was dissolved in 500 µL of chloroform or hexanes. This washing process was repeated for a total of three times with the last step being to not dissolve the QDs (left as a pellet in the tube). Next, 500 µL of DHLA and 500 µL of ethanol was added to the tube containing the pellet of QDs. A small stir bar was added and the solution was stirred at 60 °C in a water bath for 6-8 hours. After this reaction period, the solution was moved to a 15 mL Falcon tube. 4.1 mL of an ethanol/hexane/chloroform (2 mL ethanol, 2 mL hexane, 0.1 mL $CHCl_3$) mixture was added to the Falcon tube. Hexane was slowly added until the solution became turbid (2-3 mL). The turbid solution was then centrifuged for 15 minutes at 3000 x g. The supernatant was discarded and the QD pellet was dissolved in 250 µL of water. A 50K MWCO centrifugal filter was used to further purify the QDs before determining the concentration as discussed later.

A study published in ACS Nano[27] provided a possibly easier method to impart water solubility on the QDs. The QDs suspended in organic solvent was simply mixed with amphiphilic ligands in an aqueous solution, with TMAH to aid in the phase transfer between organic and aqueous phases. The biphasic solution was rapidly stirred forming an emulsion. As the native hydrophobic ligands exchanged for hydrophilic ligands the QDs move from the organic layer to the aqueous layer. The method discussed earlier, using DHLA, was eventually replaced in favor of this simpler method.

11-mercaptoundecanoic acid (MUA) was chosen as the solubilizing ligand for this experiment due its availability and ease of use. As before the QDs were thoroughly

washed prior to use using the acetone precipitation method described above. The final wash step was to dissolve the QD pellet in $CHCl_3$. A 0.5 M solution of tetramethylammonium hydroxide (TMAH) was made by dissolving 0.453 g of TMAH in 5 mL of DI water. A 0.2 M solution of MUA was made by dissolving 0.218 g of MUA in the 0.5 M TMAH solution. The MUA was dissolved in the basic TMAH solution to deprotonate the thiol and allow better binding to the QD surface[1]. Equal volumes of QDs and 0.2 M MUA were added together and vigorously stirred for 12-24 hours. Volumes anywhere from 0.5 mL to 5 mL have been successfully solubilized using this method. After stirring, the QDs moved from the lower organic layer into the aqueous layer on top as seen in Figure 1.6. The bottom organic layer was discarded and the aqueous layer then contained the QDs. The pH of the QD solution was lowered to ~8 using 0.1 M HCl, checked via pH paper. The QDs were then placed at 4 °C overnight to allow any excess MUA to precipitate out of solution. After refrigeration, the QDs were spun at 1000x g for 5 minutes to pellet any precipitated MUA. The QD supernatant was collected and the MUA pellet was discarded. To purify the QD solution, it was dialyzed using a 20k MWCO dialysis membrane against 0.1 M borate buffer (pH 8.3) for 12-24 hours with frequent dialysate changes. After purification, the concentration of the QDs was determined by UV/Vis spectrometry using the method described by Xie *et. al.*[42].

2.3 PEGylation of QDs

After water-solubilization, the surface of QDs were covered with carboxylate terminal groups from MUA surface ligands. To increase cellular uptake and reduce non-specific binding, the QDs were conjugated with poly(ethylene glycol) (PEG). Two

different PEG derivatives were conjugated to the QDs: amine-PEG-COOH ("cPEG") and amine-PEG-methoxy ("mPEG") (Figure 2.1). Primary amine terminal ends of the PEG can react with carboxylate groups on the QD surface (via MUA) to form stable amide bonds. The carboxylate terminal of the cPEG is then available for further conjugation. The methoxy terminal of the mPEG reduces the surface charge of the QD. The ratio of mPEG to cPEG can be varied to produce QDs with surface charges dependent on the intended application of the QDs. For this experiment a ratio of 1 cPEG to 5 mPEG was used. An activator (*i.e.* DMTMM) was used to allow the reaction between the terminal carboxylate groups from the QD and amine groups from the PEGs in mild aqueous conditions. Figure 2.2 shows the mechanism of DMTMM activation. The reaction of DMTMM with the QDs leaves an excellent leaving group on the QD to allow for reaction with a primary amine.

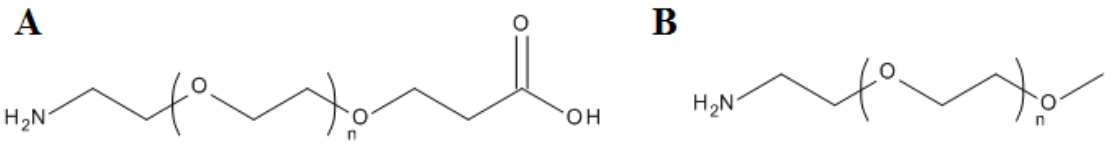

Figure 2.1. Chemical Structure of PEG derivatives. (A) amine-PEG-COOH "cPEG". (B) amine-PEG-methoxy "mPEG".

First, 1 mg/mL solutions of DMTMM, cPEG, and mPEG are prepared by weighing 1 mg of each chemical and dissolving in 1 mL of 0.1 M borate buffer, pH 8.5. Next, the DMTMM solution was added (at a 5,000 molar excess of QDs) to an Eppendorf containing water soluble QDs. The DMTMM and QDs were allowed to react for 15 minutes and then transferred to a 20k MWCO dialysis unit. The solution was dialyzed against 4 L of 0.1 M borate buffer for 15 minutes to remove any unreacted DMTMM.

This step was necessary to avoid the PEG derivatives from undergoing an intramolecular reaction. After dialysis, the activated QD solution was placed in an Eppendorf tube and solutions of mPEG and cPEG are added. The mPEG was added at a 5,000 molar excess and the cPEG is added at a 1,000 molar excess, respective to the QDs. The solution was stirred and allowed to react for 3-4 hours. Afterwards, the QDs are dialyzed again against 0.05 M borate buffer overnight to remove any excess PEGs. To ensure an accurate concentration after dialysis, the QDs were placed in a vacufuge and concentrated back to the original starting volume. Gel electrophoresis was used to determine success of the PEGylation. A 0.4% agarose gel was prepared by dissolving agarose in 0.1M borate buffer and heating until boiling. The QD-PEG conjugates and the QD precursor were electrophoresed for 30 minutes at 140 V.

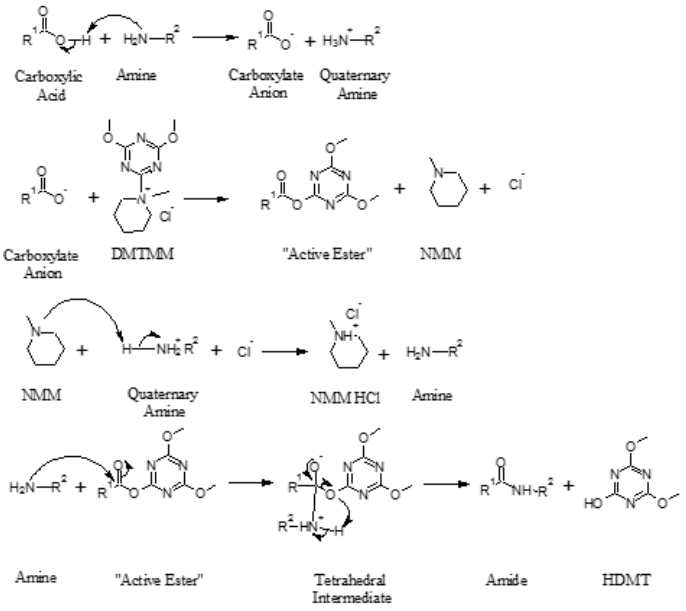

Figure 2.2. DMTMM activation mechanism[28]. Figure shows the mechanism by which DMTMM activates carboxylate groups. The activated group, shown as "active ester" is reactive toward amines in mild aqueous conditions.

2.4 Bioconjugation with Lactose

It is necessary to conjugate a targeting molecule to the QDs to direct trafficking within the cell to the desired organelle (nucleus). Once more, DMTMM was used to couple PEGylated QDs to lactose. The intended result of the reaction was a stable ester bond between terminal carboxylate groups of the PEGylated QDs and a hydroxyl group from lactose (Figure 2.3).

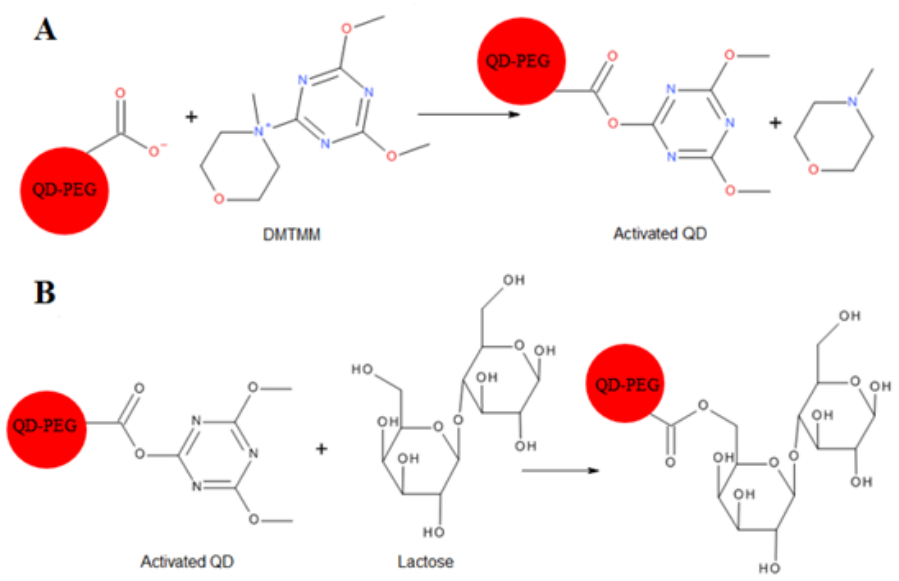

Figure 2.3. Bioconjugation of PEGylated QDs to Lactose. **A.** The PEGylated QDs are first activated with DMTMM to produce reactive intermediates. **B.** Lactose is then added and a hydroxyl group of lactose reacts with the PEGylated QDs to produce a stable ester bond. There are eight hydroxyl groups on lactose; while it is theorized primary alcohols are more reactive, it is unknown which hydroxyl reacts with the QD.

A 1 mg/mL solution of DMTMM was used to activate the carboxylate groups of the PEGylated QDs. The DMTMM was added at 5,000 molar excess to a solution of 500 nM PEGylated QDs in an Eppendorf tube and allowed to react for 15 minutes. A 5 mg/mL solution was lactose is prepared in 0.1 M borate buffer, pH 8.5, and added at

5000 molar excess with respect to the QDs. The solution was stirred and allowed to react for 4-6 hours. After the reaction was complete the solution was dialyzed in a 20k MWCO dialysis unit against 0.05 M borate buffer overnight. A vacufuge was used to concentrate the solution back to the original volume of QDs to identify QD concentration. The success of the reaction was confirmed by nuclear magnetic resonance (NMR) spectroscopy.

2.5 Imparting Positive Charge

For the QDs to able to electrostatically bind DNA they must have a positive surface charge. After water solubilization the QDs was passivated with MUA; the QD surface was negative due to the terminal carboxylate groups of MUA. Therefore, the QDs must be functionalized in a way that imparts a positive surface charge while still maintaining water solubility. The carboxylate groups on the QD surface were reacted with the diamine compound 3-(dimethylamino)-1-propylamine (DMAPA). DMAPA contains both a terminal primary amine which can be reacted with carboxylates and a terminal tertiary amine that remains unreactive under the reaction conditions. Figure 2.4 shows the reaction scheme used. As with the other reactions, DMTMM was first used to activate carboxylate groups (via MUA) on the QD surface. A 10,000 molar excess of DMTMM (relative to the QDs) was added to a 1.5 mL centrifuge tube containing 500 nM water-soluble QDs in 0.1M borate buffer, pH 8.5, and allowed to react for 15 minutes. Then, a 10,000 molar excess of DMAPA (relative to QDs), diluted to ~0.01M in 0.1M borate buffer, was added to the tube containing the QDs. The reaction was stirred for 4-6 hours and then dialyzed in a 20k MWCO dialysis unit overnight against 0.05M borate

buffer, pH 8.5. After dialysis, a vacufuge was used to concentrate the QD solution back to the starting volume. Once completed, the success of the reaction was investigated using gel electrophoresis.

Gel electrophoresis was used to determine the successful addition of DMAPA to the QD and the ability of the QD:*tert*-amine conjugates to electrostatically bind polyanionic DNA. The QD:*tert*-amine conjugates were electrophoresed through a 0.4% agarose gel containing SYBR Safe (a green fluorescing DNA dye) in 0.1M MOPS buffer (pH 7.0). The QD conjugates were incubated with pDNA (4 µL QDs to 2 µg pDNA) at room temperature for 10 minutes before loading into the gel. The samples were electrophoresed for 30 minutes at 120V and then visualized with a UV transilluminator.

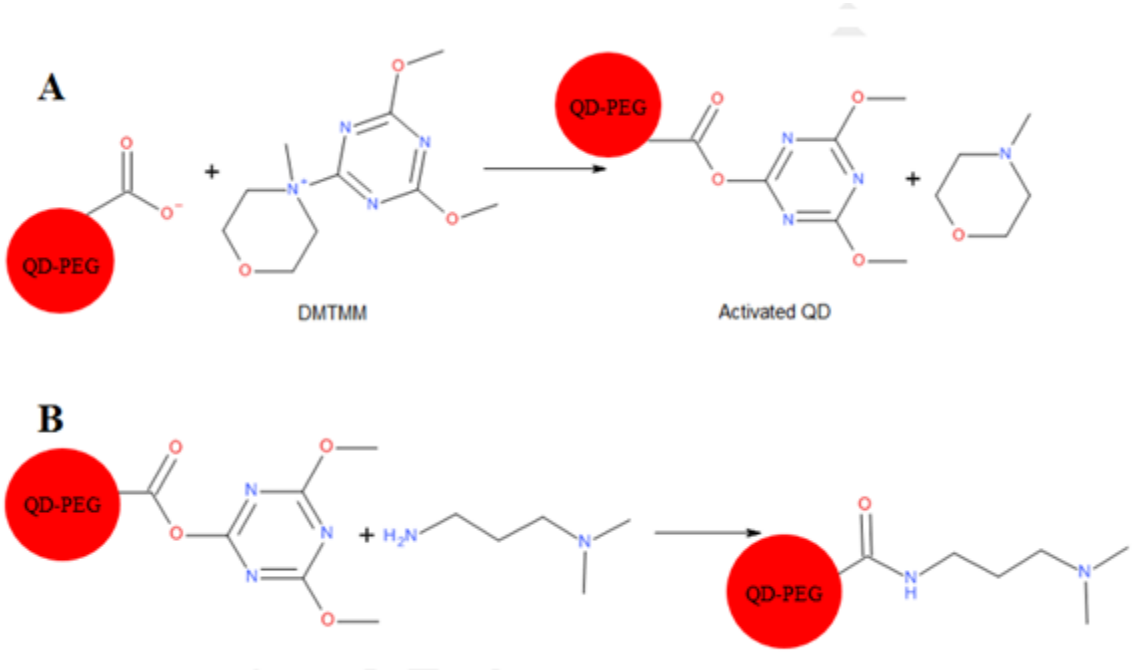

Figure 2.4. Scheme depicting the reaction of QDs with a diamine. **A.** The QDs were first activated with DMTMM. **B.** DMAPA was added and reacted with the activated carboxylate groups. The resulting reaction functionalized the surface of the QD with tertiary amines which are protonatable at physiological pH.

2.6 Immunocytochemistry and Microscopy

A model cell line of N2a cells (Mouse Neuroblastoma, ATCC Cat #HB-12317) were used to visualize the cellular trafficking of the QD-PEG-lactose conjugates. Cells were grown in media consisting of Dulbecco's Modified Eagle's Medium (DMEM) supplemented with 10% fetal bovine serum (FBS) along with antibiotic and antimitotic solution (100 units/mL Penicillin G, 100 μg/mL Streptomycin, and 0.25 μg/mL Amphotericin B). Cells were cultured and passaged every 2-3 days to prevent overcrowding within the cell culture flask.

N2a cells were plated onto 18 mm circular coverslips in a 12 well plate at a density of 40,000 cells/well and allowed to incubate for 24 hours at 37 °C in a 5% CO_2 incubator. When cells reached ~60% confluency, they were incubated with the lactosylated QDs. The lactosylated QDs were diluted in cell culture media to a final concentration of 8 nM. At this time, spent media in each well was aspirated away, replaced with media containing lactosylated QDs, and incubated at 37 °C for 8 hours. The cells were then fixed using 4% paraformaldehyde (PFA) in phosphate buffered saline (PBS) for 15 minutes. After fixing, the cells were permeabilized with 0.5% Triton X-100 for 20 minutes and then washed three times with PBS for 10 minutes. At this point, cells could be stored at 4 °C indefinitely as long as PBS did not evaporate to dry the coverslips.

Immunocytochemistry (ICC) was used to label and visualize cellular proteins using antibodies. Cellular organelles were labeled using antibodies specific for proteins that localize within that particular organelle. To visualize where lactosylated QDs localized within the cell, a variety of organelles were labeled. In this study, the organelles

labeled were nuclear envelope, Golgi body, endoplasmic reticulum (ER), lysosomes, and early endosomes (EE).

First, fixed and permeabilized cells containing lactosylated QDs were blocked with 10% bovine albumin serum (BSA) in PBS for 1 hour. Cells were then incubated with primary antibodies at the concentration recommended by the manufacture in humidified chambers overnight at 4 °C. The following day, cells were washed three times with PBS for 15 minutes and then blocked again for 1 hour with 10% BSA in PBS. The coverslips were then incubated with the secondary antibody, anti-rabbit Alexa488 (1-1000 dilution in 10% BSA in PBS), for 1 hour at room temperature. Following secondary incubation, cells were washed three times with PBS for 15 minutes and then stored in the 12 well plate with 0.1 M borate buffer, pH 8.5. The coverslips could then be placed into a magnetic imaging chamber for use in fluorescence microscopy.

Both epifluorescence and confocal microscopy were used to visualize QD conjugates with the cells. For epifluorescence microscopy, a Zeiss Axio Observer microscope equipped with a Zeiss Axiocam MRm CCD camera was used. Two sets of filter cubes were used during imaging: Rhodamine (ex545nm/em605nm) and FITC (ex470nm/em525nm) (Figure 2.5). The sets of filters in each cube allowed for visualization of each fluorophore individually (*i.e.* Alexa488 and QDs). Figure 2.6 shows the excitation/emission spectra for each fluorophore. The FITC filter cube was used to for visualizing the Alexa488-conjugated antibodies used for ICC. The rhodamine cube was used for visualizing the QD conjugates.

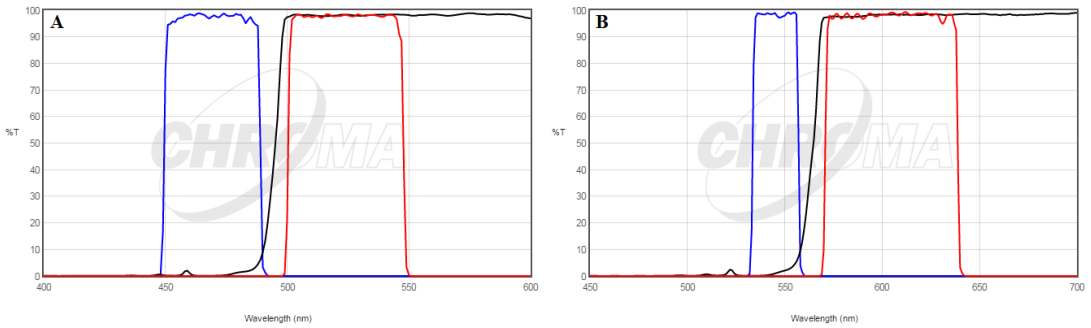

Figure 2.5. Filter cube emission and excitation cutoffs. Two filter cubes were used to visualize the cells during microscopy. (A) FITC cube – used to visualize Alexa488 conjugated antibodies. (B) Rhodamine cube – used to visualize QD conjugates.

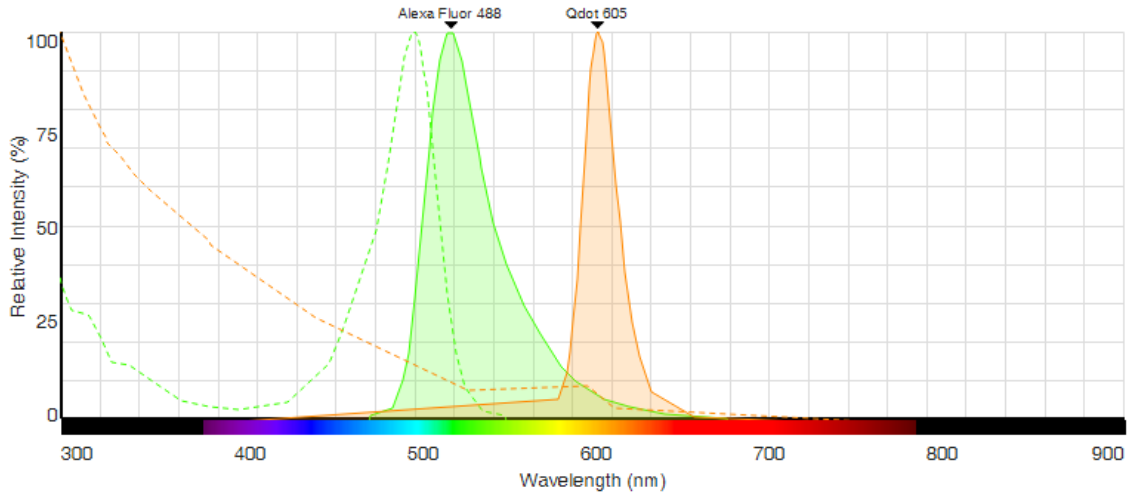

Figure 2.6. Excitation and emission of Alexa488 and QD conjugates[29]. These spectra show the excitation (dotted lines) and emission (solid lines) spectra of each fluorophore. The filter cubes used were chosen to remove any overlap between signals.

CHAPTER 3: RESULTS AND CONCLUSIONS

3.1 Water Solubilization of QDs

Early attempts at imparting water solubility to the QDs were done using dihydrolipoic acid (DHLA). The use of a bidentate ligand, in theory, should provide more stable water-soluble QDs due to the two binding sites with the QD surface. However, many trials resulted in only partial solubilization of the QDs. Some QDs became water-soluble while others remained soluble only in organic solvents, or precipitated out of solution all together. The likely cause of this incomplete transfer of QDs from organic solvent to aqueous buffer is due to oxidation of the DHLA. The two sulfhydryl groups of DHLA can be oxidized to form an intramolecular disulfide bond, resulting in the formation of lipoic acid. Lipoic acid cannot bind to the QD surface because it now lacks the sulfhydryl groups required to bind to the QD surface. The work up after solubilization was also tedious and not optimized. Different organic solvents (*i.e.* $CHCl_3$, hexanes, and ethanol) had to be added in precise amounts to cause turbidity in the sample. This method of water solubilization left a lot of room for error that resulted in incomplete solubilization of the QDs.

After solubilization trials with DHLA, 11-mercaptoundecanoic acid (MUA) was chosen as the solubilizing ligand. The MUA solubilization protocol was a simpler, more repeatable method. A solution of MUA was added to the QDs in organic solvent and stirred resulting in complete solubilization of the QDs (Figure 3.1). The concentration of MUA was optimized and 0.2 M MUA was found to work best. Less MUA resulted in

incomplete solubilization of the QDs while more resulted in excess MUA that proved difficult to remove.

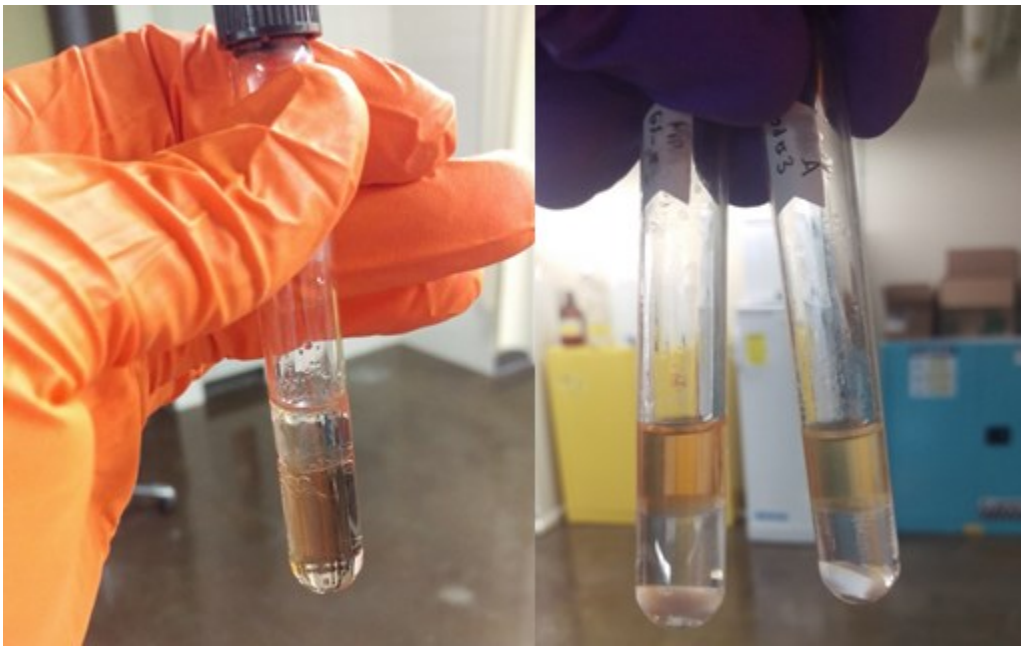

Figure 3.1. Water solubilization of QDs. These images show the successful transfer of QDs from chloroform (left image) to an aqueous solution (right image).

Once the QDs were soluble in water, some purification needed to be done to remove excess MUA from solution. After solubilization, the QD solution has a pH of ~11. Adding 0.1 M HCl to lower the pH to ~8 resulted in MUA precipitating out of solution. Unbound MUA is not very soluble in a solution below pH 10. The QDs were then placed in a refrigerator at 4 °C for several hours, allowing more MUA to precipitate from solution. Finally, dialysis overnight was used to remove any MUA left in solution.

QDs successfully solubilized by either MUA or DHLA proved to be stable in aqueous solution. Samples of MUA-solubilized QDs were stable for several months

stored at 4 °C in 0.1M borate buffer. DHLA-solubilized QDs stored at room temperature in 0.1 M borate buffer have been stable for over a year.

Previous work in our lab was used polymer encapsulated QDs. A benefit to using a ligand exchange solubilization (vs. polymer encapsulation) is a decrease in overall size. Dynamic light scattering (DLS) was used to determine the hydrodynamic radius of the water-soluble QDs. Figure 3.2 demonstrates that QDs solubilized by ligand exchange are approximately 4 nm smaller in diameter. Solubilization via ligand exchange also produced QDs that were more uniform in size (evidenced by a lower standard deviation in hydrodynamic diameter, Figure 3.2).

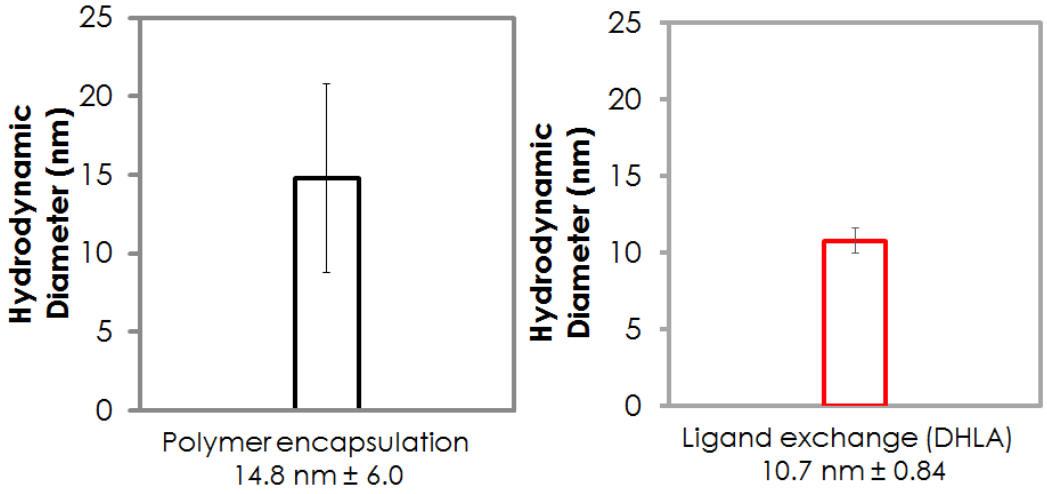

Figure 3.2. DLS size comparison between solubilization methods[30]. Solubilization via ligand exchange method produces smaller, more uniformly sized QDs as compared to polymer encapsulation.

3.2 Surface Functionalization of Water Soluble QDs

After the InP/ZnS QDs were soluble in water, the terminal carboxylate groups (via MUA) were functionalized to reduce non-specific binding and target the QD within the cell. To reduce non-specific binding both mPEG and cPEG (Figure 2.1) were

conjugated to the QDs. Addition of poly(ethylene glycol) was shown in previous work to reduce non-specific cellular interactions with the QDs[17,18]. The addition of PEG was accomplished using DMTMM as an activator, and successful PEGylation was confirmed via agarose gel electrophoresis (Figure 3.3). PEGylated QDs are larger and have a reduced surface charge due to terminal methoxy groups of mPEG; therefore, PEGylated QDs to not move as far through the gel as unconjugated QDs.

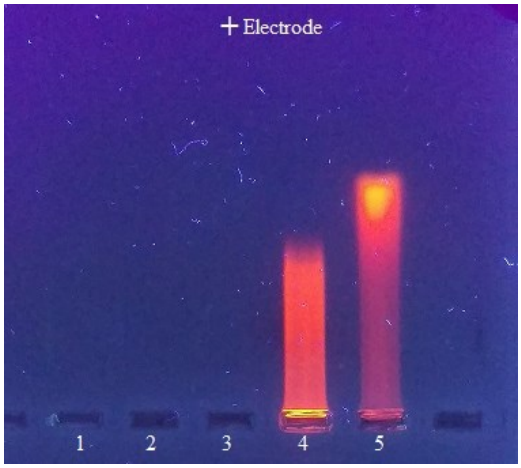

Figure 3.3. Electrophoretic characterization of PEGylated QDs. An agarose gel was used to confirm conjugation of PEG to the QDs. Lane 4 shows the PEGylated QDs and lane 5 shows unconjugated QDs. The PEGylated QDs move slower through the gel due to increased size and decreased surface charge.

Once the PEGylated QDs were confirmed via electrophoretic characterization, lactose was conjugated to terminal carboxylate groups of the QD. DMTMM was used as an activator to conjugate lactose to the QDs. Hydrogen NMR was used to confirm successful conjugation between lactose and the QDs. The peaks of the hydrogens on the anomeric carbons of lactose were used to determine successful conjugation. These peaks appear as doublets at 4.31-4.33 and 5.08-5.09 ppm, respectively (Figure 3.4). The

presence of these peaks in the NMR spectrum of the QD-lactose conjugate confirms lactosylation of PEGylated QDs (Figure 3.5).

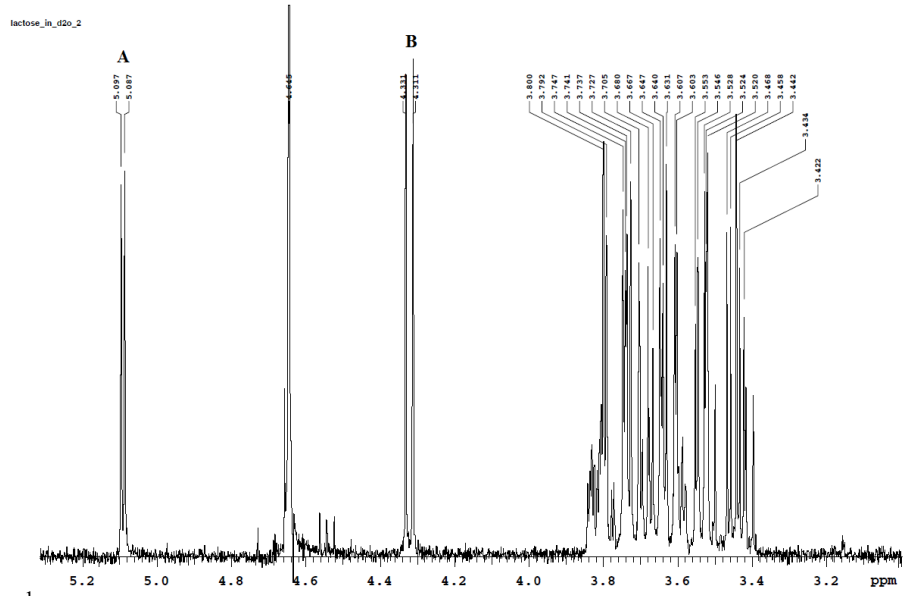

Figure 3.4. ^{1}H NMR of lactose at 400 MHz in D_2O. Peaks labeled A and B represent the hydrogens on the anomeric carbons of lactose.

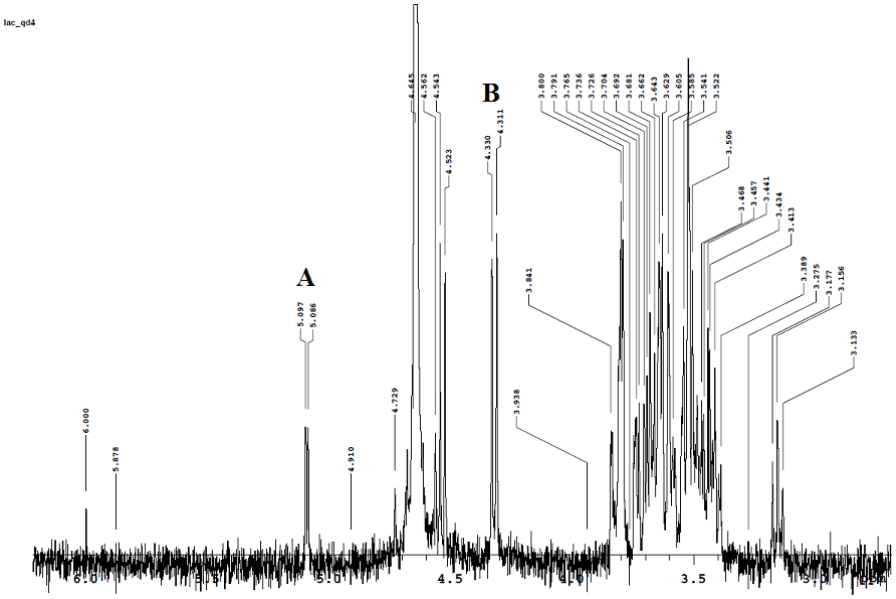

Figure 3.5. ^{1}H NMR of QD-lactose conjugates at 400 MHz in D_2O. Peaks labeled A and B depict the anomeric hydrogens of lactose, demonstrating successful conjugation of lactose to the QDs.

3.3 Imparting Positive Charge

To electrostatically interact with pDNA, the QDs must have a positive surface charge. A diamine compound, 3-(dimethylamino)-1-propylamine (DMAPA), was chosen because of its small size and presence of both primary and tertiary amino groups. The primary amine was reacted with the terminal carboxylate groups on the QD surface using DMTMM as an activator. The tertiary amine is not reactive under these conditions and is protonatable at physiological pH (~7.4), serving as a source of positive charge on the QDs. Gel electrophoresis was used to investigate the surface charge of the QD-diamine conjugates (here on referred to as "QD-*tert*-amine conjugates"). The addition of DMAPA to the QD surface was expected to impart positive surface charge on the QDs. Unconjugated QDs migrated toward the positive electrode, as expected; however, QD-*tert*-amine conjugates appeared to remain in the well (Figure 3.6). There are two possible explanations for the QD-*tert*-amine not migrating within the gel: 1) The QD-*tert*-amine conjugates aggregated to the degree that they are too large to move through the gel matrix, or 2) the QD-*tert*-amine have a neutral surface charge and therefore do not migrate toward either electrode. To test the second hypothesis, the molar ratio of DMTMM was increased in an attempt to activate additional carboxylate groups on the QD surface. In theory, if more carboxylate groups are activated, this may allow more DMAPA to react, further increasing the positive charge on the QD surface. However, this increase in the molar ratio of DMTMM caused the QDs to precipitate out of solution during the reaction. It is believed that upon activation of too many terminal carboxylate groups the QDs lose water solubility and precipitate from solution. This doesn't allow any further reaction to take place.

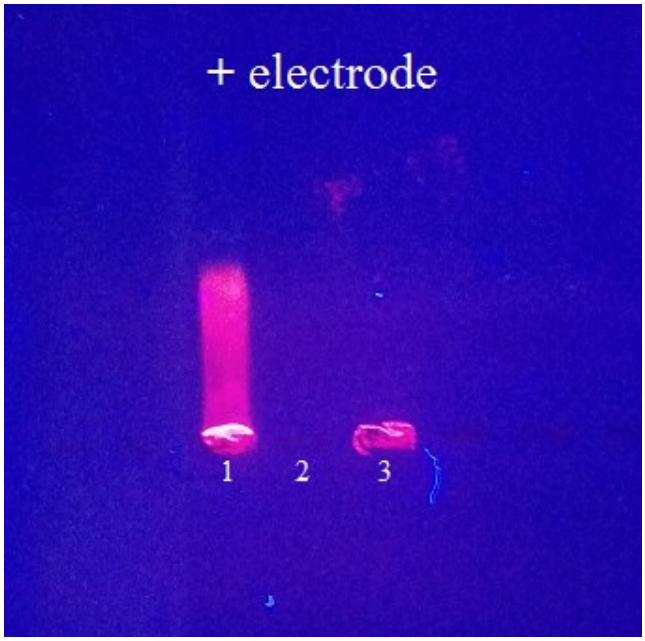

Figure 3.6. Electrophoretic characterization of QD-*tert*-amine conjugates. Lane 1 – Precursor (control) QDs. Lane 2 – Empty. Lane 3 – QD-*tert*-amine conjugates. This gel shows that the control QDs moved toward the positive electrode as expected. However, the QD-*tert*-amine conjugates remained in the well, and did not migrate toward either electrode.

Electrophoresis was used to investigate any electrostatic interaction between the QD-*tert*-amine conjugates and plasmid DNA (pDNA). The QD-*tert*-amine conjugates were incubated with pDNA for 10 minutes at room temperature and then loaded into the gel. SYBR Safe, a green fluorescent dye that intercalates DNA, was added to the agarose gel to allow visualization of the pDNA.

As expected, unconjugated QDs moved toward the positive electrode due to the negative surface charge imparted by MUA. (Figure 3.7, lane 1). Much of the QD-*tert*-amine conjugates, which were not incubated with pDNA, was retained in the well (lane 2); however, a small amount of QD-*tert*-amine conjugates appear as a faint streak toward the positive electrode, indicating at least a partial negative surface charge. In lane 3, QD-*tert*-amine conjugates incubated with pDNA, did appear to migrate from the well as well.

However, the pDNA added to the QD-*tert*-amine sample appears to have migrated independently of the QD-*tert*-amine, *i.e.* similar to the migration of pDNA alone (lane 4). The independent migration patterns in lane 3 do not indicate an interaction between the pDNA and QDs (Figure 3.7). These results seem to indicate that the surface charge of the QD is partially negatively charged and therefore is not able to electrostatically complex the pDNA.

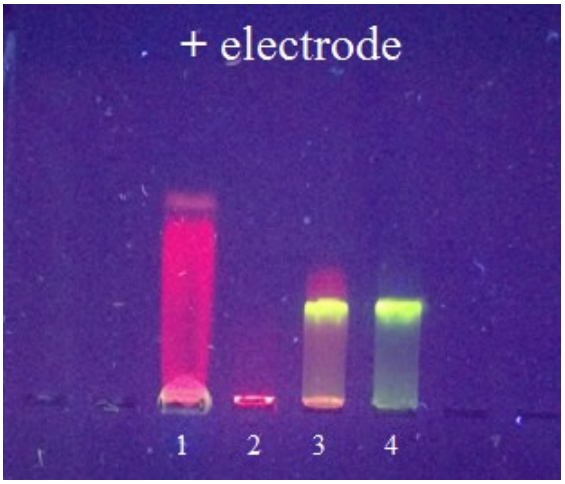

Figure 3.7. Interaction of QD-*tert*-amine and pDNA. Lane 1 – Unconjugated QDs. Lane 2 – QD-*tert*-amine. Lane 3 – pDNA and QD-*tert*-amine. Lane 4 – pDNA control. The QD-*tert*-amine and pDNA were allowed to incubate at room temperature for 10 minutes prior to loading into the gel. Lane 3 shows that the pDNA appears to not interact with the QD-*tert*-amine conjugates and migrate independently through the gel.

Attempts to increase the positive surface charge of QDs by increasing the molar ratio of DMTMM in the DMAPA reaction proved unsuccessful. The increase in DMTMM caused the QDs to precipitate from solution. This may be due to the conversion of too many carboxylate groups into the active ester intermediate during the reaction. The carboxylate groups aid the solubilization of QDs in water due to the presence of the negatively charged carboxylate groups. The activated ester (Figure 2.2) does not contain

any charged groups and may decrease water solubility causing the aforementioned precipitation of QDs during the reaction.

3.4 Cellular Trafficking of QD-Lactose Probes

To visualize trafficking of the lactosylated QDs, cells were imaged using fluorescence microscopy after performing ICC. The organelles labeled during ICC were: the Golgi apparatus, the nuclear envelope, lysosomes, and early endosomes. Control coverslips were also imaged that were treated with unconjugated QDs. Both epifluorescence and confocal microscopy were used to visualize the trafficking of QDs in the cells.

Epifluorescence microscopy was used initially to visualize cellular trafficking of the lactosylated QDs. Figures 3.8 and 3.9 show cells treated with QDs and immunolabeled for the Golgi apparatus. There appears to be some overlap between the QDs and Golgi in both cases. However, it is not possible to draw a conclusion on whether the two colocalize or not using epifluorescence microscopy. The QDs could be colocalized with the Golgi, or the QDs could be localized above or below the Golgi, due to the large width of the focal plane in epifluorescence microscopy. Figures 3.10 and 3.11 depict cells immunolabeled for the nuclear envelope, and Figures 3.12 and 3.13 depict cells immunolabeled for the lysosomes. Similar to cells with labeled Golgi apparatus, there appears to be some overlap between the labeled organelle and the QDs. To quantitatively analyze colocalization, the cells must be imaged using confocal microscopy. Confocal microscopy can be used to visualize very thin focal planes within the cells to determine colocalization.

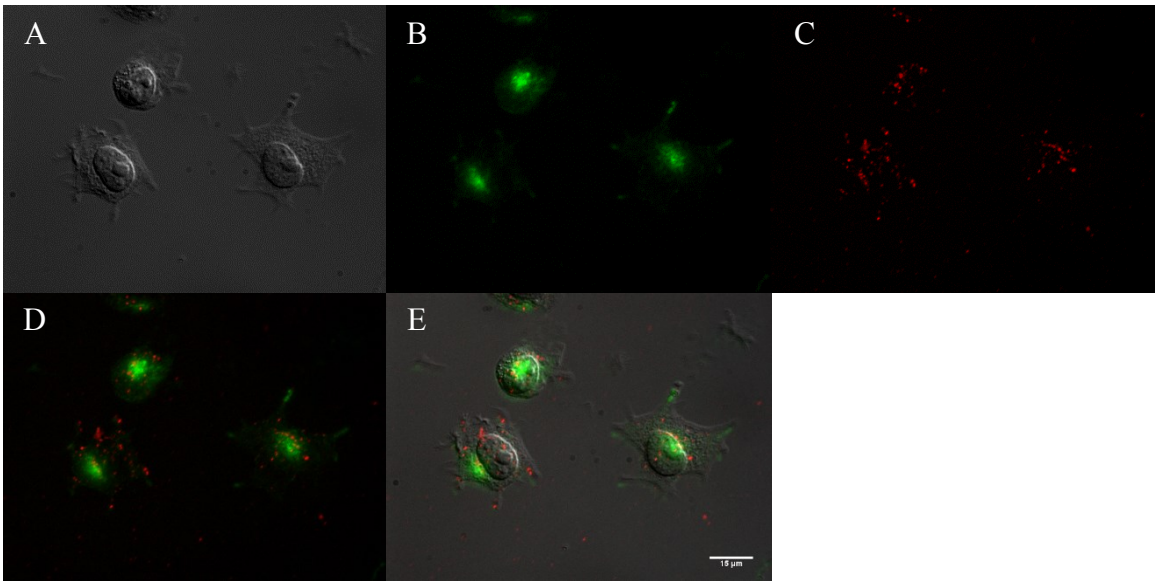

Figure 3.8. N2a cells incubated with unconjugated QDs and immunolabeled for the Golgi apparatus. These images show N2a cells incubated with 6 nM unconjugated QDs for 8 hours and immunolabeled for the Golgi apparatus. (A) DIC image of N2a cells. (B) the Golgi apparatus. (C) QDs. (D) Overlay of Golgi and QDs (E) Overlay of images A-C. Bar = 10 μm.

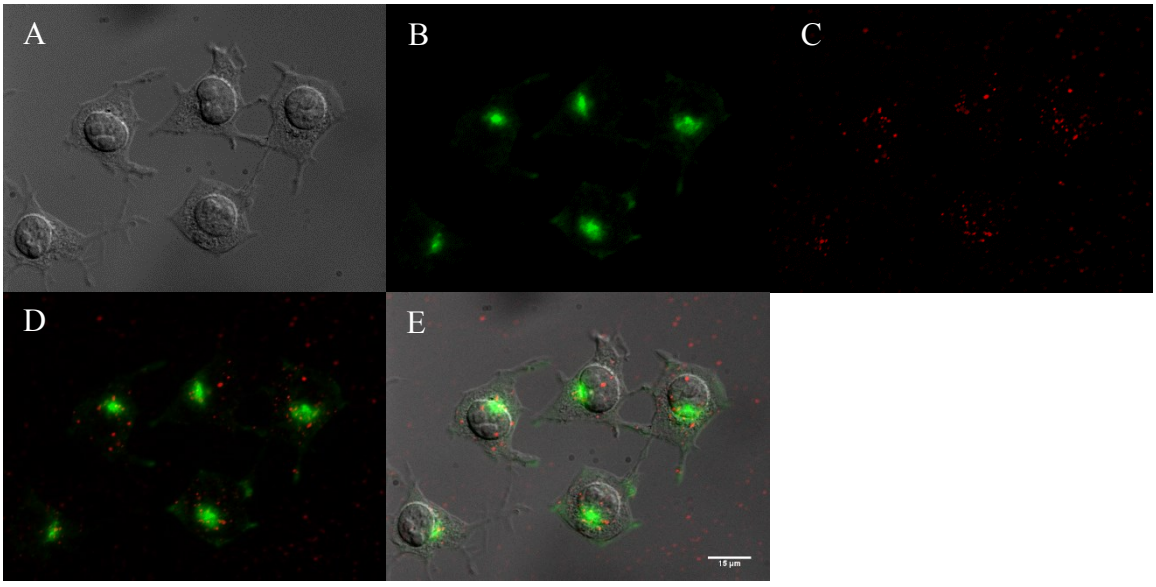

Figure 3.9. N2a cells incubated with lactosylated QDs and immunolabeled for the Golgi apparatus. These images show N2a cells incubated with 6 nM lactosylated QDs for 8 hours and immunolabeled for the Golgi. (A) DIC image of N2a cells. (B) Golgi apparatus. (C) Lactosylated QDs. (D) Overlay of Golgi and QDs. (E) Overlay of images A-C. Bar = 10 μm.

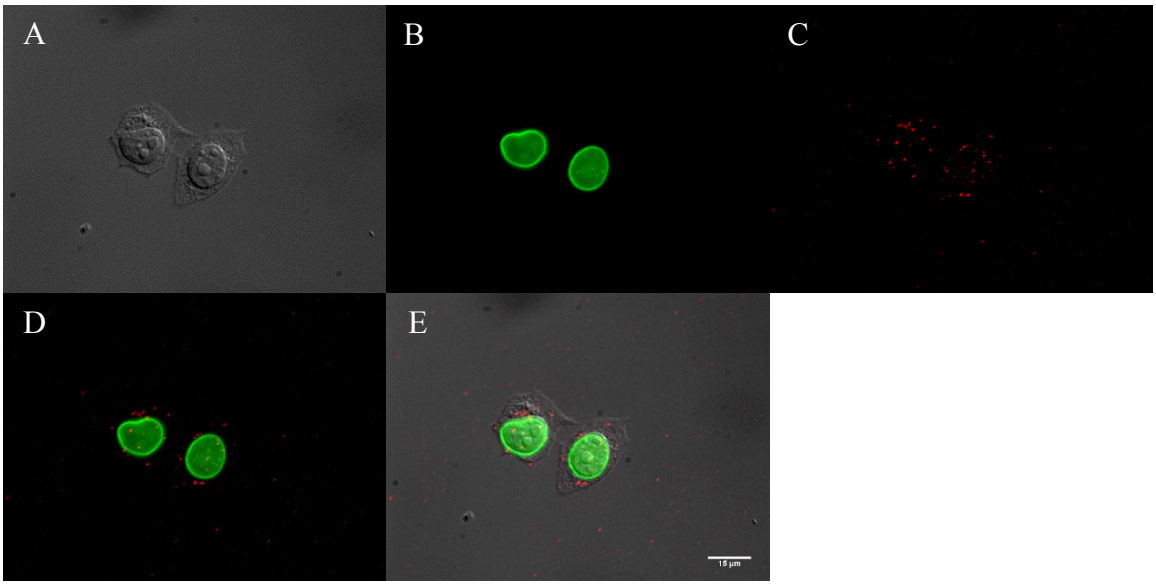

Figure 3.10. N2a cells incubated with unconjugated QDs and immunolabeled for the nuclear envelope. These images show N2a cells incubated with 6 nM unconjugated QDs for 8 hours and immunolabeled for the nuclear envelope. (A) DIC image of N2a cells. (B) Nuclear envelope. (C) QDs. (D) Overlay of nuclear envelope and QDs. (E) Overlay of images A-C. Bar = 10 µm.

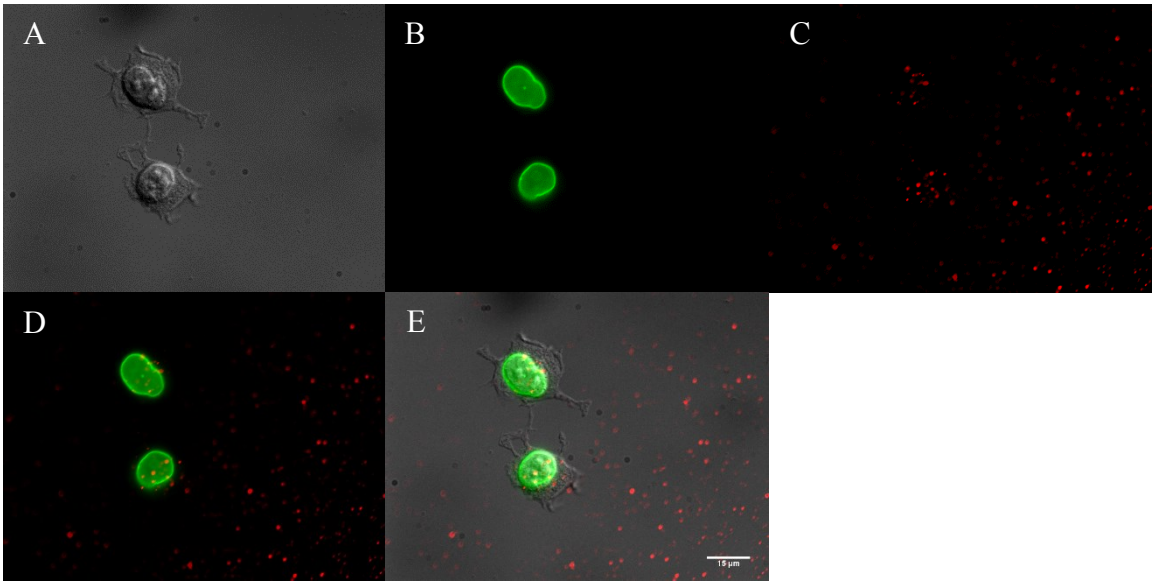

Figure 3.11. N2a cells incubated with lactosylated QDs and immunolabeled for the nuclear envelope. These images show N2a cells incubated with 6 nM lactosylated QDs for 8 hours and immunolabeled for the nuclear envelope. (A) DIC image of N2a cells. (B) FITC channel showing the nucleus. (C) Lactosylated QDs. (D) Overlay nuclear envelope and QDs. (E) Overlay of images A-C. Bar = 10 µm.

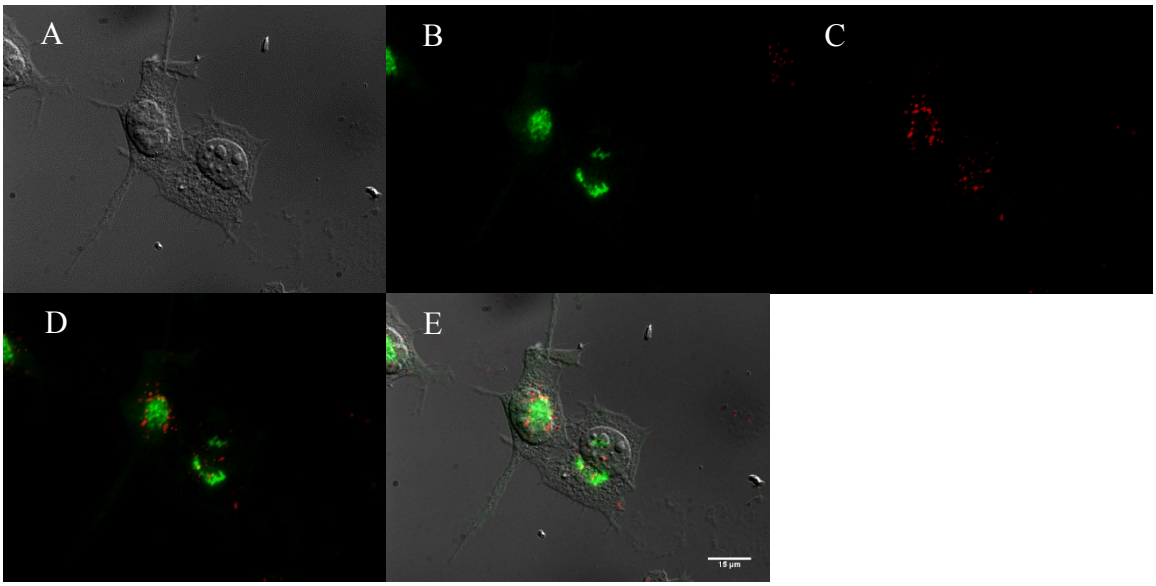

Figure 3.12. N2a cells incubated with unconjugated QDs and immunolabeled for the lysosomes. These images show N2a cells incubated with 6 nM unconjugated QDs for 8 hours and immunolabeled for the lysosomes. (A) DIC image of N2a cells. (B) Lysosomes. (C) QDs. (D) Overlay of lysosomes and QDs. (E) Overlay of images A-C. Bar = 10 µm.

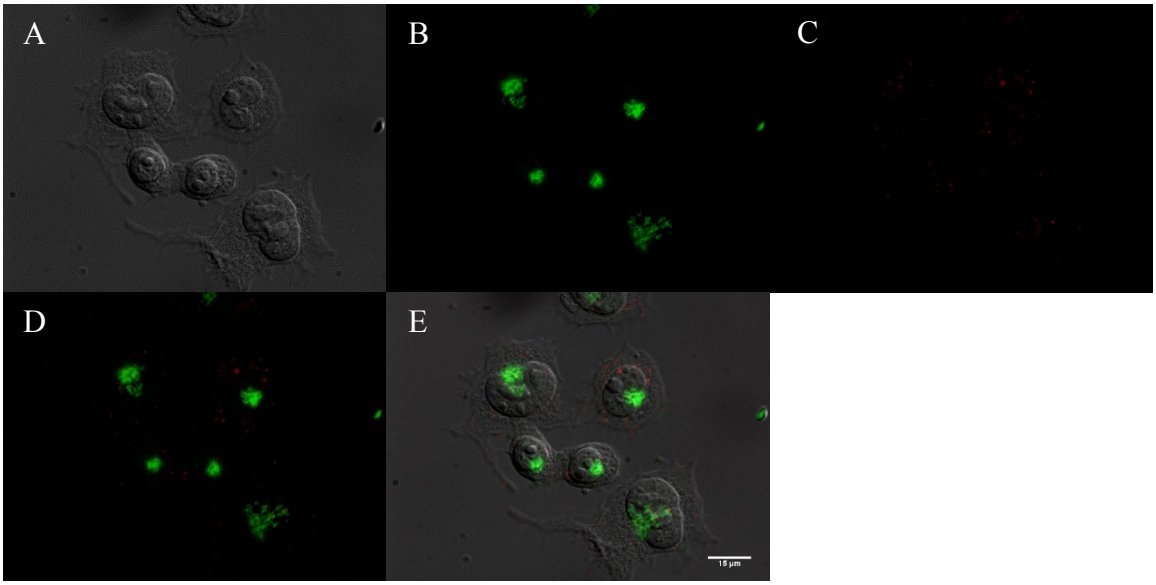

Figure 3.13. N2a cells incubated with lactosylated QDs and immunolabeled for the lysosomes. These images show N2a cells incubated with 6 nM lactosylated QDs for 8 hours and immunolabeled for the lysosomes. (A) DIC image of N2a cells. (B) Lysosomes. (C) Lactosylated QDs. (D) Overlay of lysosomes and QDs. (E) Overlay of images A-C. Bar = 10 µm.

In a second imaging experiment, ICC was used to label different cellular organelles, confocal microscopy was used to visualize trafficking of QDs within the cell, and Manders' colocalization coefficients were used to determine the overlap between the red channel (QDs) and green channel (organelles). The M1 value was examined instead of M2 because M1 focuses on red pixels (QDs) while M2 focuses on green pixels (organelle). However, upon examination of the figures, significant bleed-through from the green channel into the red channel was observed. That is, some of the signal in the red channel originated from the green fluorophore, distorting the results. Because of this bleed-through, it was not possible to accurately calculate the amount of co-localization. However, the Manders' coefficient still might hold some useful information if the amount of bleed-through was consistent for each image. If so, comparison of M1 values between cells incubated with unconjugated QDs and lactosylated QDs may indicate if the presences of lactose caused any change in QD trafficking within the cell.

A z-stack of images can be visualized by creating a what is known as a maximum projection. In generating a maximum projection, each pixel in the stack is analyzed and the pixel with the highest intensity is chosen to create the final image. Maximum projections were created (Figures 3.14 – 3.19) for each imaged cell with internalized QDs. While the maximum projection is shown here for visual purposes, the quantitative analyses described below used the entire 3-D volume of the cell (*i.e.* each slice in each stack was included in the analysis).

Manders' co-localization analysis was performed on three confocal z-stacks to calculate an M1 value. M1 values for co-localization between the QDs and the Golgi apparatus were 0.502 ± 0.009 for unconjugated QDs and 0.521 ± 0.237 for lactosylated

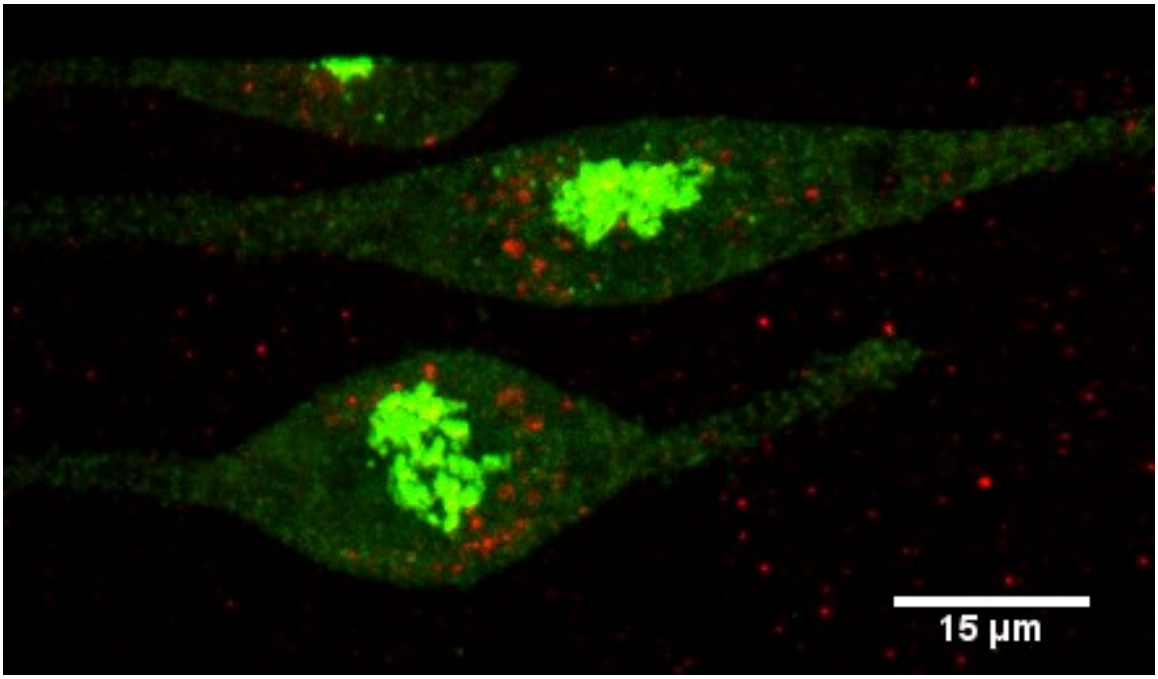

Figure 3.14. 3-D maximum project image used to investigate colocalization between the Golgi apparatus and lactosylated QDs. Green: Golgi apparatus, Red: lactosylated QDs.

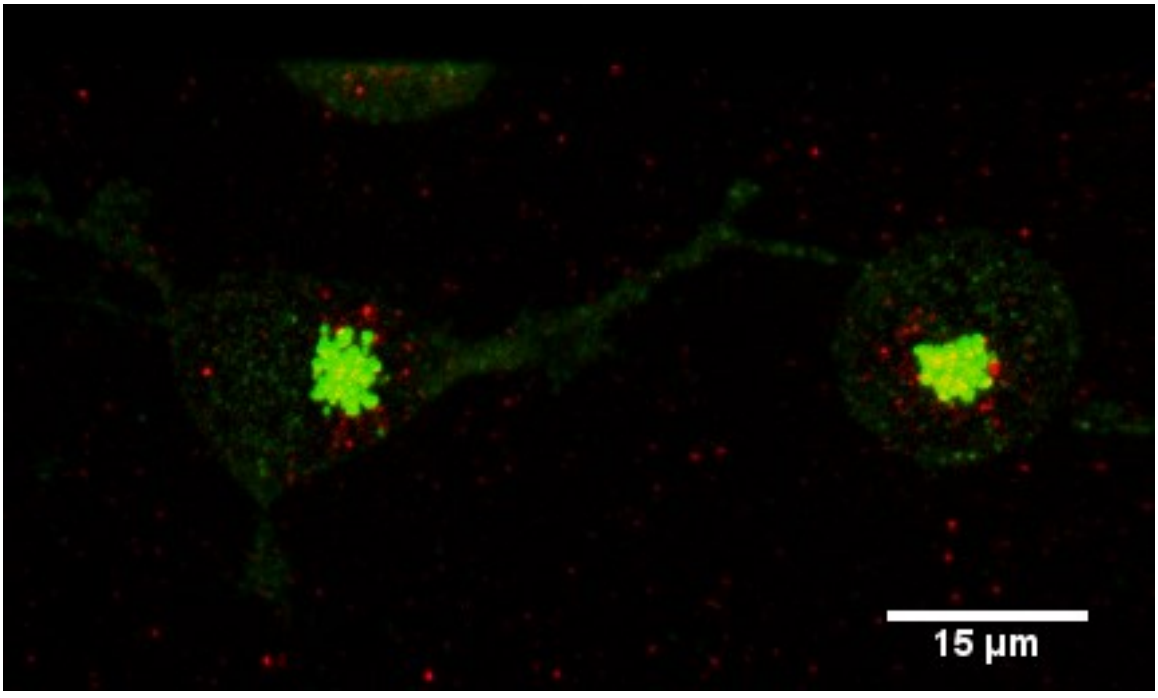

Figure 3.15. 3-D maximum project image used to investigate colocalization between the Golgi apparatus and unconjugated QDs. Green: Golgi apparatus, Red: lactosylated QDs

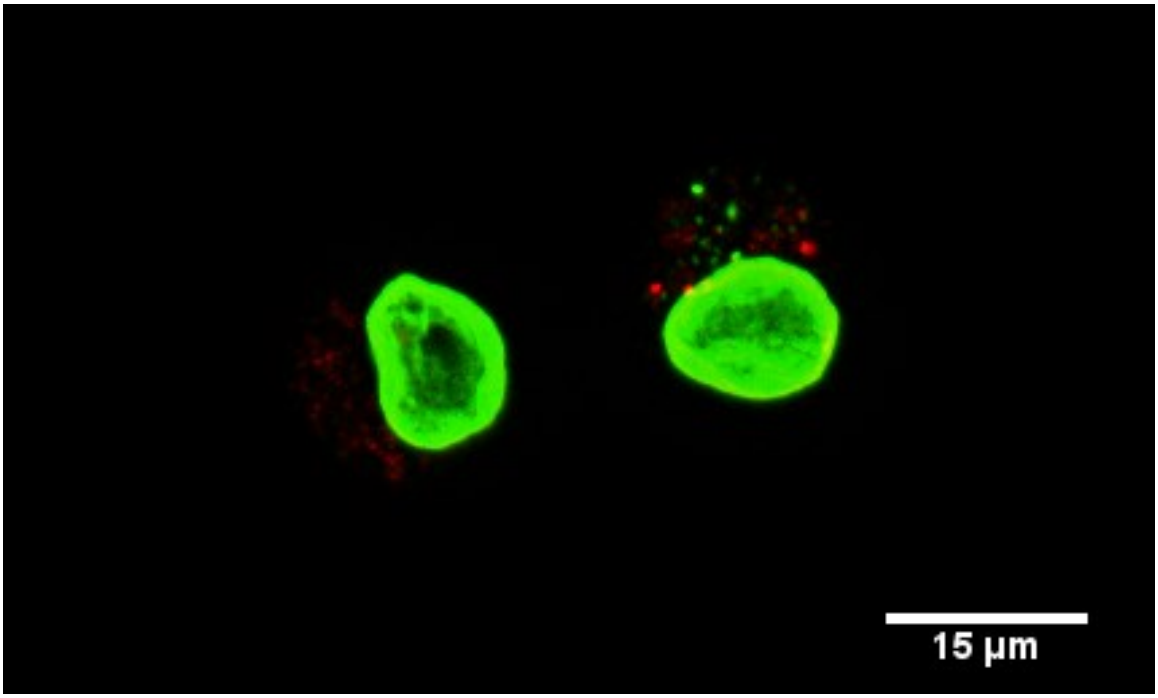

Figure 3.16. 3-D maximum project image used to investigate colocalization between the nuclear envelope and lactosylated QDs. Green: nuclear envelope. Red: QDs.

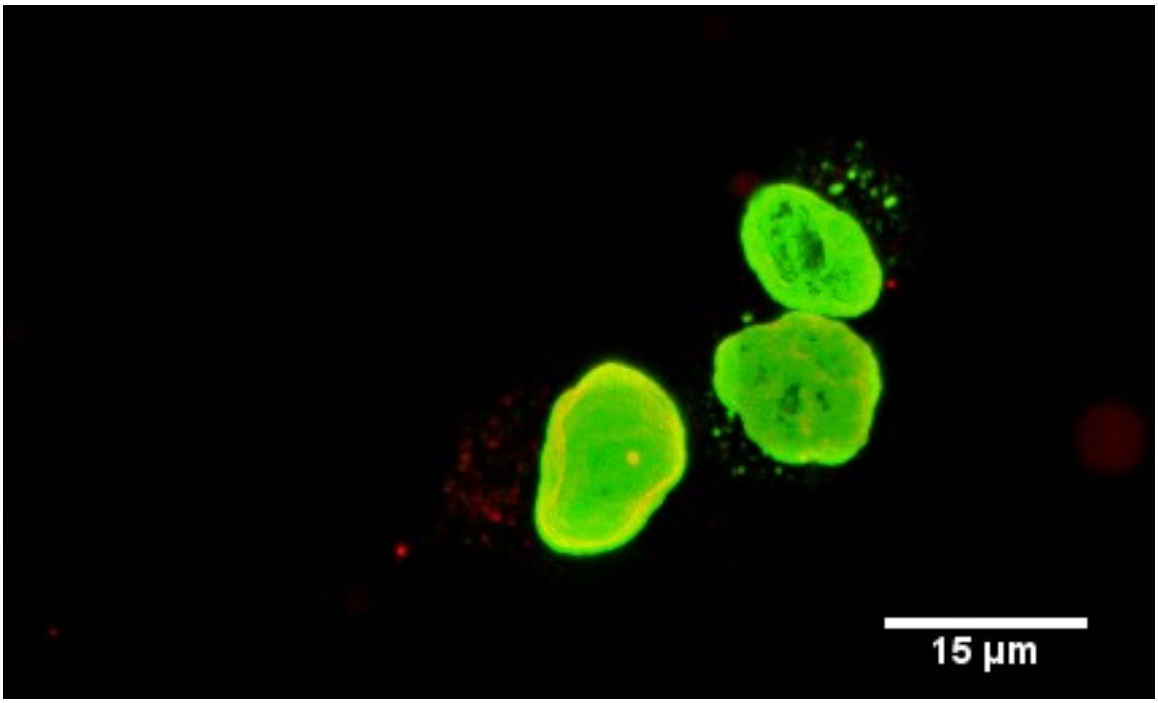

Figure 3.17. 3-D maximum project image used to investigate colocalization between the Golgi apparatus and unconjugated QDs. Green: nuclear envelope. Red: QDs.

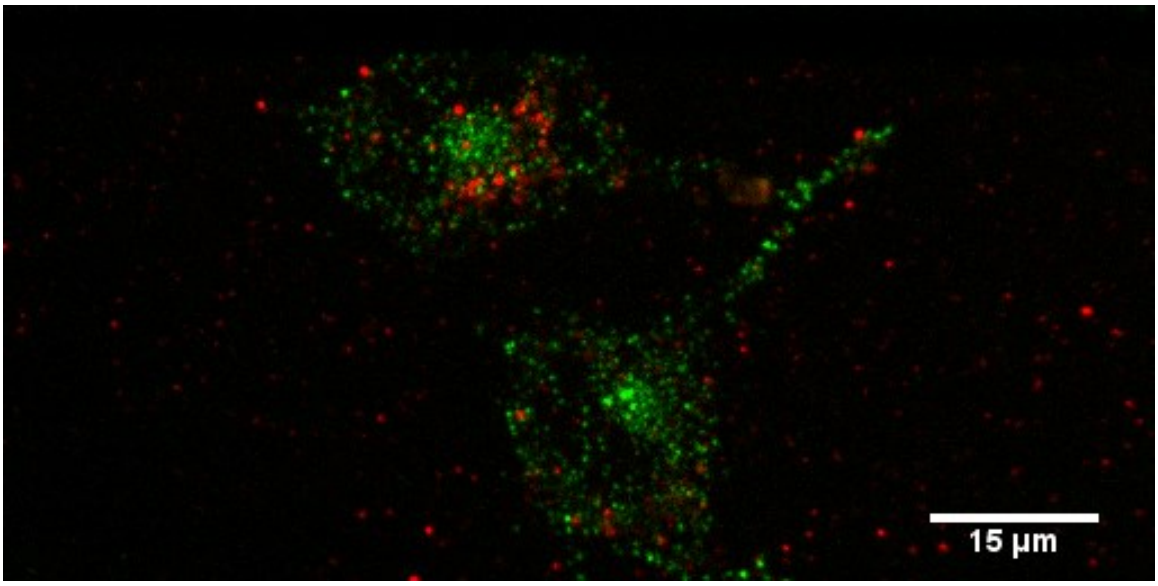

Figure 3.18. 3-D maximum project image used to investigate colocalization between the early endosomes and lactosylated QDs. Green: early endosomes. Red: QDs.

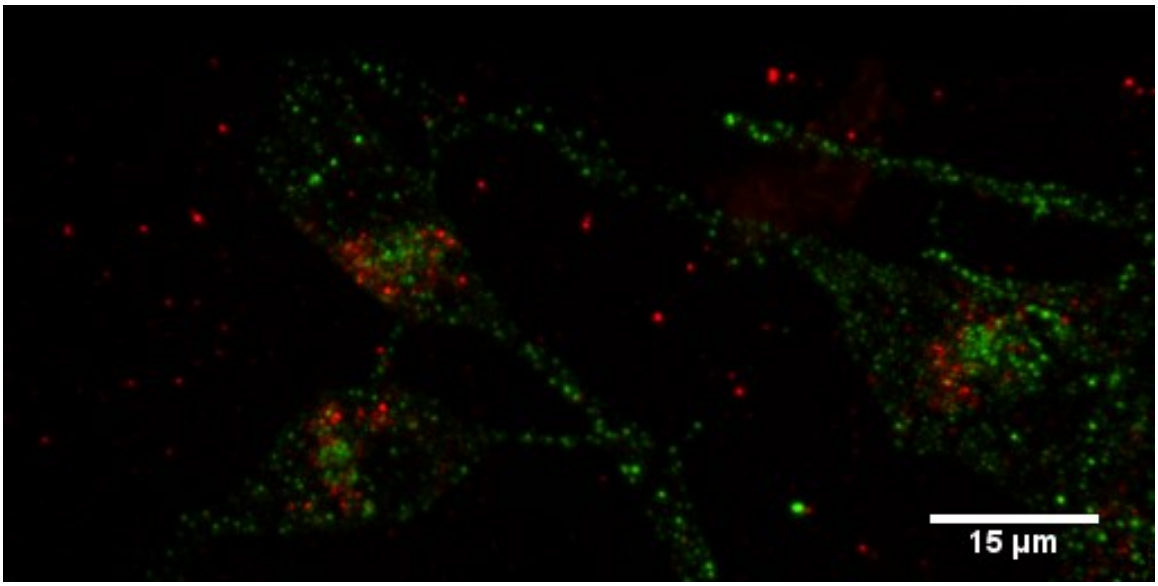

Figure 3.19. 3-D maximum project image used to investigate colocalization between the early endosomes and unconjugated QDs. Green: early endosomes. Red: QDs.

QDs (Figure 3.20). These values are too close to determine if the lactosylation of QDs caused a change in trafficking to the Golgi apparatus. M1 values for colocalization between QDs and the nuclear envelope were 0.963 ± 0.019 and 0.860 ± 0.093 for non-lactosylated and lactosylated QDs, respectively. Again, these values are too close to

accurately conclude lactose effectively targeted the QDs toward the nucleus. Manders' values for colocalization between the QDs and the early endosomes were calculated as 0.304 ± 0.083 and 0.285 ± 0.114 for the non-lactosylated and lactosylated QDs, respectively. These values also offered no further evidence that the lactosylated QDs were trafficked differently than non-lactosylated QDs.

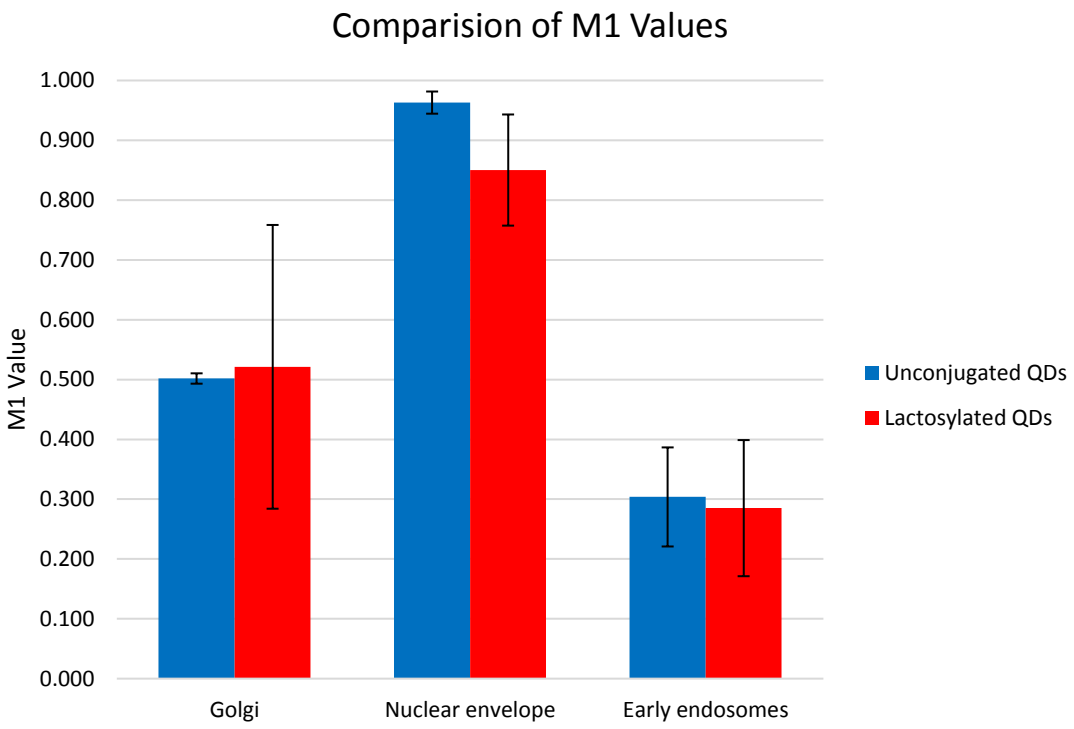

Figure 3.20. Comparison of M1 Values. Graph showing M1 values and standard deviation for each organelle.

3.5 Conclusion and Future Work

This work explored the possibility of using lactosylated QD vectors as non-viral gene therapy vectors. Initial work was successful in optimizing water solubility techniques, functionalization with PEG derivatives, and bioconjugation of lactose. The ligand exchange solubilization produced QDs that were far more stable overtime than

previously used polymer encapsulated QDs. Imparting a positive charge on the QDs proved to be more difficult than previously expected. Similar work was done in the lab previously in an attempt to impart positive charge on polymer-encapsulated QDs, but inconclusive results were obtained in attempts to functionalize QDs with positive charge using QDs solubilized with MUA. Analysis of the imaging data seems to conclude there is not difference in trafficking between the lactosylated and non-lactosylated QDs. The bleed through between the red and green channels didn't allow for conclusive colocalization to be determined. Comparison of M1 values between the lactosylated and non-lactosylated QDs, even with the bleed over, are too similar to come to a conclusion.

Further work needs to be done optimizing the diamine reactions to produce an overall positive charge on the QDs. A molecule such as poly-arginine could be used to increase the overall positive charge. Intracellular trafficking experiments were completed using both conventional and confocal microscopy but need to be revisited using a different filter combination to produce usable results.

REFERENCES

1. Talapin, D.V., Lee, J., Kovalenko, M.V., Shevchenko, E.V., Prospects of Colloidal Nanocrystals for Electronic and Optoelectronic Applications. Chem. Rev. 110, 389-458 (2010)

2. Anderson, K.E., Fong, C.Y. and Pickett, W.E., Quantum Confinement in CdSe Nanocrystallites. J. of Non-Crystalline Solids. 229-302, 1105-1110 (2002)

3. Michalet, X. et al., Quantum Dots for Live Cells, in Vivo Imaging, and Diagnostics. Science Magazine, 307, 538-544 (2008).

4. Mic´ic´, O. I., Cheong, H. M., Fu, H., Zunger, A., Sprague, J. R., Mascarenhas, A., and Nozik, A.J. Size-Dependent Spectroscopy of InP Quantum Dots. J. Phys. Chem. B, 101, 4904-4912 (1997)

5. Buhro, W.E. and Colvin, V.L. Semiconductor nanocrystals: Shape matters
Nature Materials 2, 138 - 139 (2003)

6. Sigma Aldrich, Quantum Dots, Available at http://www.sigmaaldrich.com/materials-science/nanomaterials/quantum-dots.html (2015).

7. Image obtained from http://www.rshydro.co.uk/what-is-fluorescence/Hines, D. A., Becker, M. A. & Kamat, P. V., Photoinduced Surface Oxidation and Its Effect on the Exciton Dynamics of CdSe Quantum Dots. The Journals of Physical Chemistry 116 (24), 13452-13457 (2012).

8. Hines, D. A., Becker, M. A. & Kamat, P. V., Photoinduced Surface Oxidation and Its Effect on the Exciton Dynamics of CdSe Quantum Dots. The Journals of Physical Chemistry 116 (24), 13452-13457 (2012).

9. P. Mulvaney, L. M. Liz-Marzán, M. Giersigc and T. Unga Silica encapsulation of quantum dots and metal clusters. J. Mater. Chem., 10, 1259-1270 (2000)

10. Stewart, M.H., Susumu, K., Mei, B.C., Medintz, I.L., Delehanty, J.B., Blanco-Canosa, J.B., Dawson, P.E., and Mattoussi, H. Multidentate Poly(ethylene glycol) Ligands Provide Colloidal Stability to Semiconductor and Metallic Nanocrystals in Extreme Conditions J. Am. Chem. Soc., 132 (28), 9804–9813 (2010)

11. Cavazzana-Calvo, M., Thrasher, A. & Mavilio, F., The Future of Gene Therapy. Nature 427, 779-781 (2004).

12. Yi, Y., Jong Noh, M. & Hee Lee, K., Current Advances in Retroviral Gene Therapy. Current Gene Therapy, 218-228 (2011).

13. Niidome, T., Huang, L. Gene Therapy Progress and Prospects: Nonviral vectors. Gene Therapy 9, 1647-52 (2002).

14. Zelphati, O., Nguyen, C., Ferrari, M., Felgner, J., Tsai, Y. and Felgner, PL. Stable and monodisperse lipoplex formulations for gene delivery. Gene Therapy 5, 1272–1282 (1998)

15. ThermoFisher Scientific, Cationic Lipid Mediated Transfection. From https://www.thermofisher.com/us/en/home/references/gibco-cell-culture-basics/transfection-basics/gene-delivery-technologies/cationic-lipid-mediated-delivery/how-cationic-lipid-mediated-transfection-works.html

16. Lechardeura, D., Verkmanb, A.S., and Lukacsa, G.L. Intracellular routing of plasmid DNA during non-viral gene transfer. Advanced Drug Delivery Reviews. 57 (5), 755-767 (2005)

17. Mishra, S., Paul Webster, P., Davis, M.E. PEGylation significantly affects cellular uptake and intracellular trafficking of non-viral gene delivery particles. Eur. J. Cell Biol. 83, 97-111 (2004)

18. Fichter, K. M., Zhang, L., Kiick, K. L. & Reineke, T. M., Peptide-Functionalized Poly(ethylene glycol) Star Polymers: DNA Delivery Vehicles with Multivalent Molecular Architecture. Bioconjugate Chemistry, 76-88 (2008).

19. Dagher, S., Wang, J., and Patterson, R. Identification of galectin-3 as a factor in pre-mRNA splicing. Proc. Natl. Acad. Sci. 92, 1213-1217 (1995)

20. Dumic J, Dabelic S, and Flogel M. Galectin-3: an open-ended story. Biochimica et Biophysica Acta. 1760(4), 616-635 (2006)

21. Krzeslak, A and Lipinska, A. Galectin-3 as a multifunctional protein. Cell and Molecular Biology Letters. 9, 305-328 (2004)

22. Lang, W. Nomarski differential interference-contrast microscopy (PDF). ZEISS Information. 70: 114–120 (1968)

23. Image accessed on April 15, 2017 from: https://en.wikipedia.org/wiki/File:DIC_Light_Path.png

24. Image accessed on April 15, 2017 from: https://commons.wikimedia.org/wiki/File: FluorescenceFilters_2008-09-28.svg

25. Image accessed on April 15, 2017 from: http://cam.facilities.northwestern.edu/files/2014/07/Picture-17.png

26. Dunn, K., Kamocka, M., and McDonald, J.H. A practical guide to evaluating colocalization in biological microscopy. Am J Physiol Cell Physiol. 300(4), 723-742 (2011)

27. Tamang, S., Beaune, G., Texier, I., and Reiss, P. Aqueous Phase Transfer of InP/ZnS Nanocrystals Conserving Fluorescence and High Colloidal Stability. *ACS Nano*. (5)12 9392-9402 (2011).

28. Thompson, K. F., Modification of Polymeric Substrates using Surface-Grafted Nanoscaffolds (Georgia Institute of Technology, 2005), Vol. Dissertation.

29. ThermoFisher Scientific. Available at: https://www.thermofisher.com/us/en/home/life-science/cell-analysis/labeling-chemistry/fluorescence-spectraviewer.html

30 Ellis, M. A., Grandinetti, G., Fichter, K. M. Synthesis of Cd-free InP/ZnS Quantum Dots Suitable for Biomedical Applications. *J. Vis. Exp.* (108), e53684, doi:10.3791/53684 (2016).

31 Fichter, K. M., Ingle, N. P., McLendon, M. P. & Reineke, T. M., Polymeric Nucleic Acid Vehicles Exploit Active Interorganelle Trafficking Mechanisms. *ACS Nano* **7** (1), 347-364 (2013).

32 Gerion, D., Pinaud, F., Williams, S., Parak, W., Zanchet, D., Weiss, S., and Alivisatos, P. Synthesis and Properties of Biocompatible Water-Soluble Silica-Coated CdSe/ZnS Semiconductor Quantum Dots. J. Phys. Chem. B, 105, 8861-8871 (2001)

33 Nakahara, S., Hogan, V., Inohara, H., and Avraham Raz, A. Importin-mediated Nuclear Translocation of Galectin-3. *J. Biological Chemistry.* 281, 51, 39649 – 39659 (2006)

34 Nozik, A. J., Beard, M. C., Luther, J. M., Law, M., Ellingson, R. J., and Johnson, J. C. Semiconductor Quantum Dots and Quantum Dot Arrays and Applications of Multiple Exciton Generation to Third-Generation Photovoltaic Solar Cells *Chem. Rev.,* 110 (11), 6873–6890 (2010)

35 Medintz, I., Uyeda, T., Goldman, E., and Mattoussi, H. Quantum dot bioconjugates for imaging, labelling and sensing. *Nature Materials* **4**, 435 - 446 (2005)

36 Anderson, W. The best of times, the worst of times. *Science* **288**, 627–629. (2000)

37 Fox, J. US authorities uphold suspension of SCID gene therapy. *Nat Biotechnol* **21**, 217. (2003)

38 Cavazzana-Calvo, M., Thrasher, A., and Mavilio, F. The future of gene therapy. *Nature* **427**, 779–781. (2004)

39 Smith, A. M., Ruan, G., Rhyner, M. N., Nie, S. Engineering luminescent quantum dots for in vitro molecular and cellular imaging. Annals of Biomedical Engineering. 34 (1), 3-14. (2006).

40 Derfus, A. M., Chan, W. C. W., Bhatia, S. N. Probing the cytotoxicity of semiconductor quantum dots. Nano Letters. 4 (1), 11-18. (2004).

41 Brunetti, V., et al. InP/ZnS as a safer alternative to CdSe/ZnS core/shell quantum dots: in vitro and in vivo toxicity assessment. Nanoscale. 5 (1), 307-317. (2013).

42 Xie, R. Zheng, L. Peng, X. Nucleation kinetics vs chemical kinetics in the initial formation of semiconductor nanocrystals. *JACS*. **131** (42), 15457-15466. (2009).

43 Yong, K., Ding, H., and Prasad, P. Imaging Pancreatic Cancer Using Bioconjugated InP Quantum Dots. *ACS Nano.* **3**(3) 502-510. 2009.

44 Image accessed on April 15, 2017 from: https://www.photonics.com/Article.aspx?AID=19686